

## Interface reduction with multilevel Craig–Bampton substructuring for component mode synthesis

Wu, Long; Tiso, Paolo; Van Keulen, Fred

**DOI**

[10.2514/1.J056196](https://doi.org/10.2514/1.J056196)

**Publication date**

2018

**Document Version**

Final published version

**Published in**

AIAA Journal

**Citation (APA)**

Wu, L., Tiso, P., & Van Keulen, F. (2018). Interface reduction with multilevel Craig–Bampton substructuring for component mode synthesis. *AIAA Journal*, *56*(5), 2030–2044. <https://doi.org/10.2514/1.J056196>

**Important note**

To cite this publication, please use the final published version (if applicable). Please check the document version above.

**Copyright**

Other than for strictly personal use, it is not permitted to download, forward or distribute the text or part of it, without the consent of the author(s) and/or copyright holder(s), unless the work is under an open content license such as Creative Commons.

**Takedown policy**

Please contact us and provide details if you believe this document breaches copyrights. We will remove access to the work immediately and investigate your claim.



# Interface Reduction with Multilevel Craig–Bampton Substructuring for Component Mode Synthesis

Long Wu\*

*Delft University of Technology, 2628 CD Delft, The Netherlands*

Paolo Tiso†

*Swiss Federal Institute of Technology, 8092 Zürich, Switzerland*

and

Fred van Keulen‡

*Delft University of Technology, 2628 CD Delft, The Netherlands*

DOI: 10.2514/1.J056196

Component mode synthesis is commonly used to simulate the structural behavior of complex systems. Among other component mode synthesis techniques, the Craig–Bampton method stands out for its popularity. However, for finely meshed systems featuring many components, the size of the resulting assembled system is dominated by the interface degrees of freedom. The system-level interface reduction technique aims at reducing the size of the assembled reduced model by extracting a few dominant interface modes. If the size of the interface degrees of freedom is large, the resulting problem is almost as computationally expensive as the one associated to the full model. Conversely, the local-level interface reduction technique reduces the interface of each substructure *before* assembly. In this case, the computational effort associated to the local eigenvalue problem is moderate, but issues arise when enforcing compatibility between interfaces. In this paper, the computational effort related to the interface reduction is significantly reduced by performing two variants of the multilevel Craig–Bampton reduction when the subsystems are assembled in subsets. This procedure localizes the interface reduction by applying a multilevel static condensation and eigenvalue analysis on each subset in parallel. The different interface reduction techniques are assessed on large-size realistic examples.

## Nomenclature

$B$	= signed Boolean matrix
$\mathbf{g}$	= external load vector
$H$	= number of substructures
$I$	= identity matrix
$K$	= stiffness matrix
$L$	= Boolean localization matrix
$M$	= mass matrix
$m$	= number of modal coordinates
$n$	= number of physical degrees of freedom
$\mathbf{p}$	= connecting forces vector
$\mathbf{q}$	= physical degrees of freedom vector
$U \setminus S$	= left singular vectors\diagonal singular value matrix after singular value decomposition
$V$	= number of interface sets
$X$	= Craig–Bampton reduction basis
$Z$	= number of second-level subsets when applying the multilevel interface reduction
$\gamma$	= generalized coordinates vector for Craig–Bampton subsystem
$\eta$	= modal coordinates vector
$\xi$	= unique set of generalized coordinates vector
$\Phi^I \setminus \tilde{\Phi}^{NN}$	= internal vibration modes\interface-level internal vibration modes matrix

$\tilde{\Phi}^{CC}$	= matrix of interface-level characteristic constraint modes
$\tilde{\Phi}$	= characteristic constraint modes
$\Psi^{IB} \setminus \tilde{\Psi}^{NC}$	= all constraint modes\interface-level constraint modes matrix
$\omega$	= diagonal matrix containing eigenfrequencies

## Subscripts

$CB$	= referring to matrices and vectors after applying the Craig–Bampton reduction
$\mathcal{G}$	= stacked matrices and vectors from all subsystems
$\mathcal{LL}$	= referring to matrices and vectors after applying the local-level interface reduction
$\mathcal{ML}$	= referring to matrices and vectors after applying the multilevel interface reduction
$(s)$	= pertaining to the $s$ th substructure
$SL$	= referring to matrices and vectors after applying the system-level interface reduction
$\Gamma$	= pertaining to all subsets $\Gamma_i$ assembled together
$\Gamma_i$	= pertaining to the $i$ th subsets named $\Gamma_i$

## Superscripts

$B$	= interface degrees of freedom
$B_i$	= interface degrees of freedom with respect to the interface set $B_i$
$C$	= boundary component of the interface degrees of freedom
$I$	= internal degrees of freedom
$N$	= internal component of the interface degrees of freedom

Received 3 April 2017; revision received 24 October 2017; accepted for publication 4 January 2018; published online 26 March 2018. Copyright © 2018 by the American Institute of Aeronautics and Astronautics, Inc. All rights reserved. All requests for copying and permission to reprint should be submitted to CCC at [www.copyright.com](http://www.copyright.com); employ the ISSN 0001-1452 (print) or 1533-385X (online) to initiate your request. See also AIAA Rights and Permissions [www.aiaa.org/randp](http://www.aiaa.org/randp).

\*Ph.D. Researcher, Faculty of Mechanical, Maritime and Materials Engineering, Mekelweg 2; L.Wu-1@tudelft.nl.

†Senior Scientist, Institute for Mechanical Systems, Leonhardstrasse 21; ptiso@ethz.ch.

‡Full Professor, Faculty of Mechanical, Maritime and Materials Engineering, Mekelweg 2.

## I. Introduction

A SYSTEM consisting of multiple components can be modeled efficiently with proper component mode synthesis (CMS) techniques. In CMS, the dynamics of a substructure is described by a truncated set of vibration modes of each subsystem combined with a

set of static modes accounting for the coupling with neighboring subcomponents [1]. The classic Craig–Bampton (CB) method was first proposed in [2,3] and then simplified in [4,5]. It combines the concepts of componentwise analysis and modal reduction techniques, and it is one of the well-known CMS technologies. In the CB method, the coupling at an interface is realized by using a set of constraint modes (CMs) and retaining all degrees of freedom (DOFs) at the interface. However, the size of the CB basis may be dominated by the CM's DOFs if the finite element (FE) mesh is sufficiently fine. Obviously, this limits the achievable reduction, and hence decreases the efficiency of the substructuring approach. In this context, a proper interface reduction technique is a must to bring the reduction basis to a manageable size.

In 1977, Craig and Chang [6] proposed three interface reduction methods by applying either a Guyan, Ritz, or modal reduction at the interface. Castanier et al. [7] rediscovered the modal reduction techniques by using a secondary eigenvalue analysis to the interface partition of the CB system and proposing the commonly used system-level characteristic constraint (SCC) modes. This technique was applied after the system-level matrices were constructed. Consequently, it did not offer flexibility for design runs because the SCC modes must be recomputed for all the interface DOFs even if a design change occurs at a single substructure. To bring the interface reduction to a substructure level, Hong et al. [8] recently formulated the interface reduction by generating the local-level characteristic constraint (LCC) modes from mass and stiffness matrices associated to the interface DOFs before assembly. The local-level interface reduction simplified the eigenvalue problem by neglecting the coupling between neighboring subcomponents. For specific systems where the stiffness of adjacent substructures was significantly different, an undeformed interface reduction [9] could also be applied by assuming that the interface underwent only rigid-body motions.

Most of the interface reduction techniques mentioned here were developed for the CB method, owing to its wide application in CMS problems. Tran [10,11] indicated that the interface reduction techniques could be implemented with the CB method, as well as various free or hybrid interface mode-based substructuring techniques, like the CMS method proposed by MacNeal [12] and later by Rubín [13]. The interface reduction idea could also be applied to the dual CB method proposed by Rixen [14,15]. For large-scale structures with multiple interfaces, Aoyama and Yagawa [16] introduced an optional reduction method by analyzing the eigenmodes from adjacent subcomponents to reduce the computational cost. Interface reduction has also been efficiently extended to the CB approach for acoustic-structure coupled fluid-filled piping systems [17]. Balmès applied the generalized constraint modes, which were linear combinations of the constraint modes, to provide a compatible model with an optimal selection of the generalized constraint modes [18]. This idea could be further extended to the system design process as shown in [19]. Bennighof and Lehoucq [20] proposed the automatic multilevel substructuring (AMLS) method, which was a multilevel extension of the CMS substructuring based on the sparsity of the system matrices. The AMLS method was widely applied in the field of applied mathematics by recursively applying the Gaussian block elimination and modal condensation of the system matrices [21–23]. Besides all the reduction methods using “interface modes,” an alternative method called double modal synthesis [24,25] could also be applied to compensate the modal truncation. The double modal synthesis was further used to analyze brake squeal in [26]. The extension of the current interface reduction techniques to geometrical nonlinear domain remains a relevant topic. Recently, Sinou and Besset [27] extended the double modal synthesis to study the self-excited vibrations and time analysis of brake squeal in a nonlinear region. Kuether et al. [28,29] recently proposed a nonintrusive model order reduction technique by applying the system-level interface reduction. The authors' current efforts are directed to extend classic CB methods with both system-level interface reduction and modal derivatives (first proposed in [30]) for problems characterized by distributed geometric nonlinearities.

For linear systems, the system-level [7] and local-level [8] interface reduction methods are two of the most commonly used

techniques for the CMS problem due to their easy implementation and applicability. The system-level interface reduction can be computationally expensive when the number of interface DOFs is large. On the other hand, the local-level counterpart reduces the computational effort by localizing the interface reduction at each substructure. However, the interface compatibility will be compromised if the independent reduction basis for each subsystem is inadequate. In this paper, we present two variants of the multilevel interface reduction method. We assemble the substructures into localized subsets. A secondary CB substructuring procedure is then applied in each subset. In the first variant, a secondary CB reduction is applied to the interface DOFs of the subset only, whereas in the second variant, the CB reduction is performed on all the DOFs of the subset. As opposed to the local-level method, the proposed approach does not simplify the interface coupling. Therefore, it is able to get accurate approximation as compared to system-level interface reduction methods while enabling computational savings by setting smaller subsets and the possibility for parallelization for interface reduction.

This paper is organized as follows: In Sec. II, the classic CB method is briefly introduced. The subcomponents are assembled in a primal manner, i.e., a unique set of interface DOFs is defined. In Sec. III, the existing system-level and local-level interface reduction techniques proposed in [7,8] are summarized and evaluated. Section IV presents two multilevel interface reduction variants, which were discussed previously. A computational complexity analysis is presented in Sec. V, and the advantages of the proposed approach are discussed and compared to the SCC and LCC mode-based methods. In Sec. VI, representative numerical examples are investigated. Discussions and conclusions are provided in Sec. VII.

## II. Classic Craig–Bampton Method and Primal Assembly

In this section, we first briefly outline the CB method [4] for subcomponents. Then, the subcomponents are assembled in a primal manner [31] by choosing a unique set of interface DOFs. For a linear undamped system composed of  $H$  subsystems, the equations of motion (EOMs) of the global system with *uncoupled* substructures can be written in a block-diagonal format as

$$M_{\mathcal{G}}\ddot{\mathbf{q}}_{\mathcal{G}} + K_{\mathcal{G}}\mathbf{q}_{\mathcal{G}} = \mathbf{g}_{\mathcal{G}} + \mathbf{p}_{\mathcal{G}} \quad (1)$$

where the subscript  $\mathcal{G}$  indicates that the vectors and matrices of all subsystems are stacked for the entire system by stating

$$\begin{aligned} M_{\mathcal{G}} &= \text{diag}(M_{(1)}, \dots, M_{(H)}), & \mathbf{q}_{\mathcal{G}} &= \text{col}(\mathbf{q}_{(1)}, \dots, \mathbf{q}_{(H)}), \\ K_{\mathcal{G}} &= \text{diag}(K_{(1)}, \dots, K_{(H)}), & \mathbf{g}_{\mathcal{G}} &= \text{col}(\mathbf{g}_{(1)}, \dots, \mathbf{g}_{(H)}), \\ \mathbf{p}_{\mathcal{G}} &= \text{col}(\mathbf{p}_{(1)}, \dots, \mathbf{p}_{(H)}) \end{aligned}$$

where  $M_{(s)}$  and  $K_{(s)}$  are the constant mass and stiffness matrices; and  $\mathbf{g}_{(s)}$ ,  $\mathbf{p}_{(s)}$ , and  $\mathbf{q}_{(s)}$  are the external load vector, the connecting load vector imposed by neighboring subsystems, and the generalized nodal DOFs vector of the  $s$ th decoupled subcomponent, respectively. Here,  $\text{diag}(\dots)$  and  $\text{col}(\dots)$  indicate block diagonal and column stacking, respectively.

### A. Craig–Bampton Method

Let us focus on the  $s$ th subsystem. The nodal DOFs  $\mathbf{q}_{(s)}$  in the  $s$ th subsystem can be partitioned into internal DOFs  $\mathbf{q}_{(s)}^I \in \mathbb{R}^{n_{(s)}^I}$  and boundary DOFs  $\mathbf{q}_{(s)}^B \in \mathbb{R}^{n_{(s)}^B}$  with  $n_{(s)}^I + n_{(s)}^B = n_{(s)}$ .

The CB transformation is a linear combination of constraint modes

$$\Psi_{(s)}^{I/B} \in \mathbb{R}^{n_{(s)}^I \times n_{(s)}^B}$$

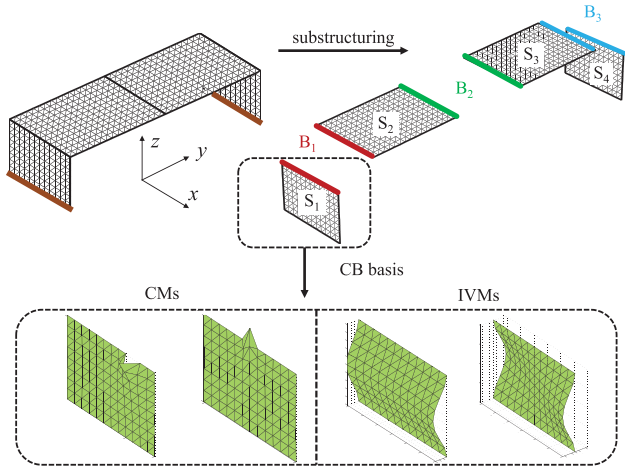


**Fig. 1** Illustration of the CB reduction on a  $\pi$ -shaped FE model composed of four substructures.

and internal vibration modes (IVMs)

$$\Phi_{(s)}^{II} \in \mathbb{R}^{n_{(s)} \times m_{(s)}}$$

by stating

$$\mathbf{q}_{(s)} = \begin{bmatrix} \mathbf{q}_{(s)}^B \\ \mathbf{q}_{(s)}^I \end{bmatrix} = \begin{bmatrix} \mathbf{I}_{(s)}^{BB} & \mathbf{0} \\ \Psi_{(s)}^{IB} & \Phi_{(s)}^{II} \end{bmatrix} \begin{bmatrix} \mathbf{q}_{(s)}^B \\ \boldsymbol{\eta}_{(s)}^I \end{bmatrix} \triangleq \mathbf{X}_{(s)} \boldsymbol{\gamma}_{(s)} \quad (2)$$

where  $\boldsymbol{\eta}_{(s)}^I$  is the vector of modal coordinates with respect to the IVMs, and  $\mathbf{X}_{(s)}$  and  $\boldsymbol{\gamma}_{(s)}$  are the CB reduction matrix and corresponding generalized coordinate vector of the  $s$ th subsystem.

To illustrate the concept, we consider here a  $\pi$ -shaped model composed of four substructures ( $S_1$  to  $S_4$ ) connected through three interfaces ( $B_1$  to  $B_3$ ), as shown in Fig. 1. The model is fixed at the bottom ( $z = 0$ ). The CMs and IVMs for each substructure can be calculated independently.

With Eq. (2), we generate a projection basis for the  $s$ th substructure, where the interface DOFs  $\mathbf{q}_{(s)}^B$  are retained without reduction. The reduced EOMs for the substructure are obtained via a classic Galerkin projection, and they are expressed by

$$\underbrace{\begin{bmatrix} \tilde{\mathbf{M}}_{(s)}^{BB} & \tilde{\mathbf{M}}_{(s)}^{BI} \\ \tilde{\mathbf{M}}_{(s)}^{IB} & \mathbf{I}_{(s)}^{II} \end{bmatrix}}_{\tilde{\mathbf{M}}_{(s)}} \begin{bmatrix} \ddot{\mathbf{q}}_{(s)}^B \\ \dot{\boldsymbol{\eta}}_{(s)}^I \end{bmatrix} + \underbrace{\begin{bmatrix} \tilde{\mathbf{K}}_{(s)}^{BB} & \mathbf{0} \\ \mathbf{0} & \omega_{(s)}^2 \end{bmatrix}}_{\tilde{\mathbf{K}}_{(s)}} \begin{bmatrix} \mathbf{q}_{(s)}^B \\ \boldsymbol{\eta}_{(s)}^I \end{bmatrix} = \underbrace{\begin{bmatrix} \tilde{\mathbf{g}}_{(s)}^B \\ \tilde{\mathbf{g}}_{(s)}^I \end{bmatrix}}_{\tilde{\mathbf{g}}_{(s)}} + \begin{bmatrix} \mathbf{p}_{(s)}^B \\ \mathbf{0} \end{bmatrix} \quad (3)$$

where  $\omega_{(s)}^2$  is the diagonal matrix containing the eigenvalues of the retained IVMs. For all the details, one should refer to the original paper [4].

### B. Primal Assembly of Component Models

The CB transformations [Eq. (2)] for each substructure can be collected for the entire system in a block-diagonal form by stating  $\mathbf{q}_G = \mathbf{X}_G \boldsymbol{\gamma}_G$ , where  $\mathbf{X}_G = \text{diag}(\mathbf{X}_{(1)}, \dots, \mathbf{X}_{(H)})$  is a block-diagonal matrix consisting of all substructure CB reduction matrices, and  $\boldsymbol{\gamma}_G = \text{col}(\boldsymbol{\gamma}_{(1)}, \dots, \boldsymbol{\gamma}_{(H)})$  is the assembled set of the generalized coordinates of subsystems for the global system.

Classically, the subcomponents are assembled in a primal manner [31]; i.e., a new reduced set of generalized coordinates of the assembled system  $\boldsymbol{\xi}_{CB}$  for the CB model is defined here as

$$\boldsymbol{\xi}_{CB} = \text{col}(\mathbf{q}_{CB}^B, \boldsymbol{\eta}_{CB}^I), \quad \text{with} \quad \boldsymbol{\eta}_{CB}^I = \text{col}(\boldsymbol{\eta}_{(1)}^I, \dots, \boldsymbol{\eta}_{(H)}^I) \quad (4)$$

where  $\mathbf{q}_{CB}^B \in \mathbb{R}^{n_{CB}^B}$  consists of the unique choice of all interface DOFs  $\text{col}(\mathbf{q}_{(1)}^B, \dots, \mathbf{q}_{(H)}^B)$ , and

$$\boldsymbol{\eta}_{CB}^I \in \mathbb{R}^{m_{CB}^I}$$

contains the internal generalized coordinates of all the substructures. For internal vibration modes, it holds that

$$m_{CB}^I = \sum_{s=1}^{s=H} m_{(s)}^I$$

The compatibility condition ensures no relative motion between the boundaries of connected substructures. The final primal EOMs for the coupled system can be written as

$$\underbrace{L_{CB}^T \mathbf{X}_G^T \mathbf{M}_G \mathbf{X}_G L_{CB}}_{\tilde{\mathbf{M}}_{CB}} \ddot{\boldsymbol{\xi}}_{CB} + \underbrace{L_{CB}^T \mathbf{X}_G^T \mathbf{K}_G \mathbf{X}_G L_{CB}}_{\tilde{\mathbf{K}}_{CB}} \boldsymbol{\xi}_{CB} = \underbrace{L_{CB}^T \mathbf{X}_G^T \mathbf{g}_G}_{\tilde{\mathbf{g}}_{CB}} \quad (5)$$

where  $L_{CB}$  is the primal assembly operator, and the connected force vectors from neighboring systems are eliminated to satisfy the force equilibrium condition. The reduced-order model (ROM) in Eq. (5) is denoted as CB-ROM. The detailed derivation of Eq. (5) can be found in [1].

The assembled matrices and vectors  $\tilde{\mathbf{M}}_{CB}$ ,  $\tilde{\mathbf{K}}_{CB}$ , and  $\tilde{\mathbf{g}}_{CB}$  can be further partitioned, corresponding to the interface coordinates  $\mathbf{q}_{CB}^B$  and internal coordinates  $\boldsymbol{\eta}_{CB}^I$ . The reduced EOMs [Eq. (5)] are therefore rewritten in a partitioned style as

$$\begin{bmatrix} \tilde{\mathbf{M}}_{CB}^{BB} & \tilde{\mathbf{M}}_{CB}^{BI} \\ \tilde{\mathbf{M}}_{CB}^{IB} & \mathbf{I}_{CB}^{II} \end{bmatrix} \begin{bmatrix} \ddot{\mathbf{q}}_{CB}^B \\ \dot{\boldsymbol{\eta}}_{CB}^I \end{bmatrix} + \begin{bmatrix} \tilde{\mathbf{K}}_{CB}^{BB} & \mathbf{0} \\ \mathbf{0} & \omega_{CB}^2 \end{bmatrix} \begin{bmatrix} \mathbf{q}_{CB}^B \\ \boldsymbol{\eta}_{CB}^I \end{bmatrix} = \begin{bmatrix} \tilde{\mathbf{g}}_{CB}^B \\ \tilde{\mathbf{g}}_{CB}^I \end{bmatrix} \quad (6)$$

where  $\omega_{CB}^2 = \text{diag}(\omega_{(1)}^2, \dots, \omega_{(H)}^2)$ . The detailed formulation of the partitioned matrices  $\tilde{\mathbf{M}}_{CB}^{BB}$  and  $\tilde{\mathbf{K}}_{CB}^{BB}$  can be found in [31], and they will be not discussed here.

If the finite element mesh is sufficiently fine and many subcomponents with distributed interfaces are considered, the size of these reduced system-level matrices is dominated by the interface DOFs. Although the number of DOFs is aggressively reduced, the sparsity of the matrices is lost. The computational gain will thus be limited. To overcome this problem, interface reduction can be applied such that truly compact models can be obtained.

## III. System-Level and Local-Level Interface Reduction Methods

The interface reduction techniques aim to reduce the size of the CB model by decreasing the number of interface DOFs. In principle, the interface reduction techniques can be applied on both a substructure level as well as on an assembly level. In this section, the commonly used interface reduction techniques on the system level [7] and substructure level [8] will be briefly discussed.

### A. System-Level Interface Reduction

The system-level interface reduction was first proposed in [6] and was further discussed in [7,18,32]. As a starting point, we recall the assembled EOMs in Eq. (6) for the CB models. By fixing the internal DOFs for all subcomponents, we obtain

$$\tilde{\mathbf{M}}_{CB}^{BB} \ddot{\mathbf{q}}_{CB}^B + \tilde{\mathbf{K}}_{CB}^{BB} \mathbf{q}_{CB}^B = \tilde{\mathbf{g}}_{CB}^B \quad (7)$$

where

$$\tilde{\mathbf{M}}_{CB}^{BB} \in \mathbb{R}^{n_{CB}^B \times n_{CB}^B}, \quad \tilde{\mathbf{K}}_{CB}^{BB} \in \mathbb{R}^{n_{CB}^B \times n_{CB}^B}$$

are the interface partition of the assembled mass and stiffness matrices in Eq. (6). This equation is used to find the interface

behavior. Hence, the interface modes can be computed from a secondary eigenvalue analysis of Eq. (7) as

$$(\tilde{K}_{CB}^{BB} - \tilde{\omega}_j^2 \tilde{M}_{CB}^{BB}) \tilde{\phi}_j = \mathbf{0}, \quad j = 1, \dots, n_{CB}^B \quad (8)$$

where the system-level characteristic constraint modes

$$\tilde{\Phi}_{SC} \in \mathbb{R}^{n_{CB}^B \times m_{SC}^B}$$

are defined here as a truncated set of the eigenvectors as

$$\tilde{\Phi}_{SC} = [\tilde{\phi}_1, \dots, \tilde{\phi}_{m_{SC}^B}]$$

with

$$m_{SC}^B \ll n_{CB}^B$$

The corresponding eigenvalues can be rewritten in diagonal matrix as

$$\tilde{\omega}_{SC}^2 = \text{diag}(\tilde{\omega}_1^2, \dots, \tilde{\omega}_{m_{SC}^B}^2)$$

Castanier et al. [7] suggested that the number of interface DOFs could be reduced by using this new set of SCC modes, where a single SCC mode represented more global motion at the interface as opposed to constraint modes. Depending on the frequency range of interest, the SCC modes could be used to generate a new CMS model with the significantly reduced number of DOFs. By taking a selected set of SCC modes, the interface DOFs were approximated by stating

$$\mathbf{q}_{CB}^B = \tilde{\Phi}_{SC} \boldsymbol{\eta}_{SC}^B$$

Essentially, the interface dominant behavior is given by the low-frequency vibration modes obtained by Guyan reduction [33].

The final EOMs by applying the system-level interface reduction techniques can be expressed as

$$\underbrace{\begin{bmatrix} I_{SC}^{BB} & (\tilde{\Phi}_{SC})^T \tilde{M}_{CB}^{BI} \\ \tilde{M}_{CB}^{IB} \tilde{\Phi}_{SC} & I_{CB}^I \end{bmatrix}}_{\tilde{M}_{SC}} \begin{bmatrix} \ddot{\boldsymbol{\eta}}_{SC}^B \\ \ddot{\boldsymbol{\eta}}_{CB}^I \end{bmatrix} + \underbrace{\begin{bmatrix} \tilde{\omega}_{SC}^2 & \mathbf{0} \\ \mathbf{0} & \omega_{CB}^2 \end{bmatrix}}_{\tilde{K}_{SC}} \begin{bmatrix} \boldsymbol{\eta}_{SC}^B \\ \boldsymbol{\eta}_{CB}^I \end{bmatrix} = \underbrace{\begin{bmatrix} (\tilde{\Phi}_{SC})^T \tilde{\mathbf{g}}_{CB}^B \\ \tilde{\mathbf{g}}_{CB}^I \end{bmatrix}}_{\tilde{\mathbf{g}}_{SC}} \quad (9)$$

where the SCC modes  $\tilde{\Phi}_{SC}$  are assumed to be mass normalized, and the assembled stiffness matrix is now fully diagonal. The ROM in Eq. (9) is denoted as SL-ROM.

For illustration, the first two SCC modes of the  $\pi$ -shaped model are shown in Fig. 2. The SCC modes exhibit a global rotation and translation at the interface DOFs. The internal DOFs follow the motion statically, as dictated by the deformation at the interface. The gray color denotes statically condensed mesh. The main advantage of this method lies in the fact that the interface compatibility across coupled substructures is still exactly enforced. However, the system-level reduction bears two major drawbacks. First, the stiffness and mass matrices ( $\tilde{K}_{CB}^{BB}$  and  $\tilde{M}_{CB}^{BB}$ ) are no longer sparse after the static condensation. Second, because the SCC modes are obtained after the system-level matrices are constructed, the SCC modes must be recomputed for all the interface DOFs, even if a design modification is performed for a single substructure. Therefore, for a large-scale system with multiple interface connections, the solution of the eigenvalue problem [Eq. (8)] is expensive when considering the large size of interface DOFs.

### B. Local-Level Interface Reduction

An alternative way to achieve interface reduction was proposed in [8] and named the ‘‘local-level reduction.’’ We briefly summarize the method in this section. We start with the reduced equation of motion [Eq. (3)] for the  $s$ th substructure. By fixing the internal DOFs  $\boldsymbol{\eta}_{(s)}^I$ , we get

$$\tilde{M}_{(s)}^{BB} \ddot{\mathbf{q}}_{(s)}^B + \tilde{K}_{(s)}^{BB} \mathbf{q}_{(s)}^B = \tilde{\mathbf{g}}_{(s)}^B + \mathbf{p}_{(s)}^B \quad (10)$$

As for the system-level case, the local interface reduction technique is also based on a secondary eigenvalue analysis of the free vibration of each substructure. In this case, the interaction with neighboring subcomponents is simply neglected by setting  $\mathbf{p}_{(s)}^B = \mathbf{0}$ . This results in the eigenvalue problem:

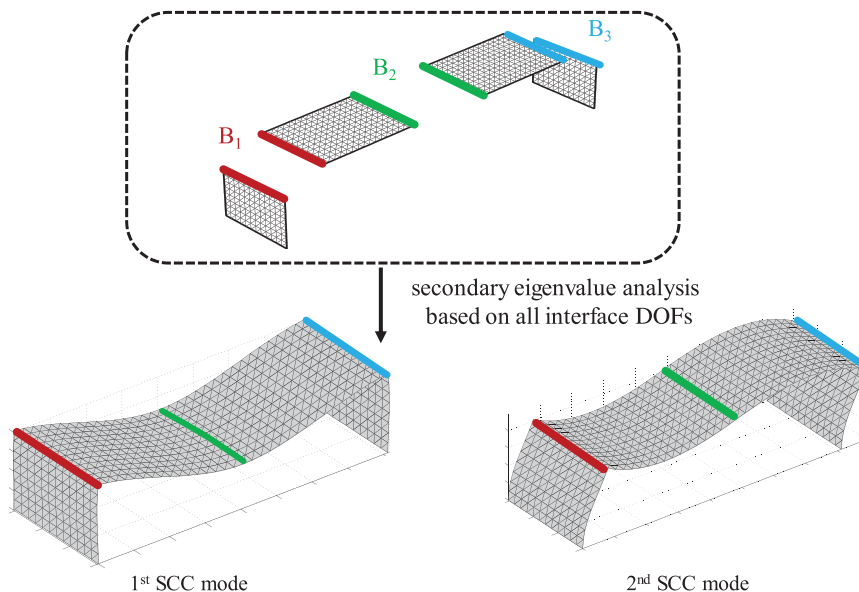


Fig. 2 First two SCC modes for the  $\pi$ -shaped FE model.

$$\left(\tilde{K}_{(s)}^{BB} - \tilde{\omega}_{j,(s)}^2 \tilde{M}_{(s)}^{BB}\right) \tilde{\phi}_{j,(s)} = \mathbf{0}, \quad j = 1, \dots, n_{(s)}^B \quad (11)$$

where a truncated set of the eigenvectors

$$\tilde{\Phi}_{\mathcal{L}\mathcal{L},(s)} \in \mathbb{R}^{n_{(s)}^B \times m_{(s)}^B}$$

called the local-level characteristic constraint modes is collected as

$$\tilde{\Phi}_{\mathcal{L}\mathcal{L},(s)} = \left[ \tilde{\phi}_{1,(s)}, \dots, \tilde{\phi}_{m_{(s)}^B,(s)} \right]$$

with

$$m_{(s)}^B \ll n_{(s)}^B$$

The LCC modes  $\tilde{\Phi}_{\mathcal{L}\mathcal{L},(s)}$  are used to reduce the interface DOFs for each substructure in a local sense.

Because the LCC modes are calculated without the knowledge of adjacent substructures, the subcomponent-level interface reduction may result in nonconforming interfaces and may cause so-called interface locking if the reduction basis is inadequate and enforces only weak compatibility between the substructures [34]. Therefore, it is important to solve the compatibility problems during the assembly step.

According to the method proposed by Hong et al. [8], the LCC modes of each interface, denoted as  $\tilde{\Phi}_{\mathcal{L}\mathcal{L}}^{B_i}$  for the interface  $B_i$ , are simply combined from connecting substructures. Take, for instance, the  $\Pi$ -shaped structure in Fig. 3:  $\tilde{\Phi}_{\mathcal{L}\mathcal{L}}^{B_1}$  contains  $\tilde{\Phi}_{\mathcal{L}\mathcal{L},(1)}^{B_1}$  and  $\tilde{\Phi}_{\mathcal{L}\mathcal{L},(2)}^{B_1}$ . This augmented set of LCC modes is used as the reduction basis for the interface of every connected substructure. This guarantees that the interface dynamics of each connected substructure are well described, at the cost of increasing the size of the basis. As an example, the  $\Pi$ -shaped model is again used to illustrate the procedure; see Fig. 3. The LCC modes are shown in different colors at the interface DOFs for each substructure. The gray mesh indicates that the internal DOFs are statically condensed. The LCC modes of each interface are simply combined from all the connecting subcomponents.

Due to the simple combination of multiple interface sets from different subsystems, the resulting reduction basis may contain linearly dependent vectors. To prevent ill conditioning, the basis should be orthogonalized. This can be achieved by performing a further singular value decomposition (SVD) for each interface  $B_i$  as

$$\mathbf{U}^{B_i} \mathbf{S}^{B_i} (\mathbf{D}^{B_i})^T = \tilde{\Phi}_{\mathcal{L}\mathcal{L}}^{B_i} \quad (12)$$

where  $\mathbf{U}^{B_i}$  and  $\mathbf{S}^{B_i}$  are the left singular vectors and diagonal singular value matrix for interface  $B_i$ . In Hong et al.'s work [8], only the left

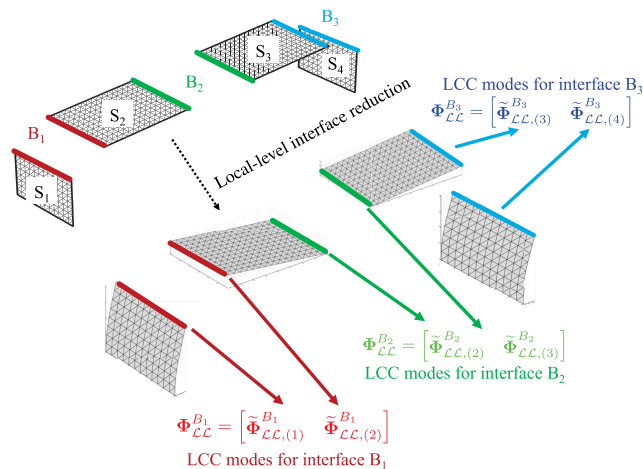


**Fig. 3** Local-level interface reduction technique [8] for the  $\Pi$ -shaped model.

singular vectors corresponding to singular values larger than 0.01% of the maximum singular value are kept, and they are placed in  $\mathbf{U}_{\mathcal{L}\mathcal{L}}^{B_i}$ . This yields the final reduction basis for all the interface DOFs as

$$\mathbf{q}_{CB}^B = \text{diag}\left(\mathbf{U}_{\mathcal{L}\mathcal{L}}^{B_1}, \dots, \mathbf{U}_{\mathcal{L}\mathcal{L}}^{B_V}\right) \cdot \text{col}\left(\boldsymbol{\eta}_{B_1}, \dots, \boldsymbol{\eta}_{B_V}\right) \triangleq \mathbf{U} \boldsymbol{\eta}_{\mathcal{L}\mathcal{L}}^B \quad (13)$$

where the subscript  $V$  is the number of interface sets. The detailed assembly procedure can be found in [8], which was complemented with a clear example. The final reduced equation of motion can be obtained by substituting the interface reduction [Eq. (13)] to the assembly of CB equations [Eq. (6)] as

$$\underbrace{\begin{bmatrix} \mathbf{U}^T \tilde{M}_{CB}^{BB} \mathbf{U} & \mathbf{U}^T \tilde{M}_{CB}^{BI} \\ \tilde{M}_{CB}^{IB} \mathbf{U} & \mathbf{I}_{CB}^I \end{bmatrix}}_{\tilde{M}_{\mathcal{L}\mathcal{L}}} \begin{bmatrix} \ddot{\boldsymbol{\eta}}_{\mathcal{L}\mathcal{L}}^B \\ \ddot{\boldsymbol{\eta}}_{CB}^I \end{bmatrix} + \underbrace{\begin{bmatrix} \mathbf{U}^T \tilde{K}_{CB}^{BB} \mathbf{U} & \mathbf{0} \\ \mathbf{0} & \omega_{CB}^2 \end{bmatrix}}_{\tilde{K}_{\mathcal{L}\mathcal{L}}} \begin{bmatrix} \boldsymbol{\eta}_{\mathcal{L}\mathcal{L}}^B \\ \boldsymbol{\eta}_{CB}^I \end{bmatrix} = \begin{bmatrix} \mathbf{U}^T \tilde{\mathbf{g}}_{CB}^B \\ \tilde{\mathbf{g}}_{CB}^I \end{bmatrix} \quad (14)$$

where the ROM in Eq. (14) is denoted as LL-ROM.

The a priori interface reduction on the subcomponent level is easy to accomplish, without knowledge of the adjacent substructures. Moreover, the eigenvalue problem associated to the LCC modes is of limited size, and therefore computationally cheap. However, because the interface behavior is dependent on all components to which it is connected, the local-level interface reduction may give far less accurate results than the system-level interface reduction because it cannot properly account for the coupling between connecting subsystems.

#### IV. Multilevel Interface Reduction

To combine the accurate system-level approach with the computationally efficient local-level method, we present two reduction methods based on a multilevel CB structuring for the local subset. Each subset is a collection of some adjacent (but not all) substructures for the entire system. This procedure localizes the interface reduction by applying a multilevel static condensation and eigenvalue analysis on interface DOFs of local subsets and, as opposed to traditional local-level techniques, does not compromise the compatibility at interfaces. In practice, it is often the case that, within the same organization, different subcomponent models have to be assembled first into larger subsystems. Next, they are joined with other subsystems developed by different organizations. The multilevel approach we propose nicely fits this scenario.

The process can be summarized in the following steps:

1) The global system is divided into substructures. For every substructure, a classical CB reduction basis is obtained, for which the interface DOFs are fully retained and the internal DOFs are reproduced by a combination of CMs and IVMs. This step has been explained in Sec. II.A.

2) We group the reduced CB models of the substructures into second-level subsets; the subcomponents within each subset are assembled in parallel at this stage. For each subset, the total DOFs can be partitioned into three sets: a) internal components of the interface DOFs (denoted as NDOFs), which have been used to connect the subsystems categorized in the same subset; b) boundary components of the interface DOFs (denoted as CDOFs), which will be connected with the neighboring subsets; and c) internal DOFs, which correspond to the modal coordinates of IVMs for the subsystems within the same subset, denoted here as IDOFs. To further reduce the size of system matrices in each subset, two multilevel ROMs, named ML1-ROM and ML2-ROM, have been proposed here. They are specifically described as follows:

a) Regarding the ML1-ROM, for each subset, a secondary CB reduction is performed for the interface DOFs (CDOFs and NDOFs). More specifically, the NDOFs are treated as the internal

component of the secondary CB reduction, and thus replaced by a truncated set of modal coordinates. The CDOFs are treated as the interface component of the secondary CB reduction, and therefore retained for exact interface compatibility during the subset assembly in the next step.

b) Regarding ML2-ROM, for each subset, a secondary CB reduction is performed for all DOFs (CDOFs, NDOFs, and IDOFs) within the subset. Although CDOFs are the interface component of the secondary CB reduction, both NDOFs and IDOFs are the internal component of the secondary CB reduction, and therefore are further reduced.

3) The subsets are coupled together using the primal assembly. It is worth noticing that step 2 can be applied recursively in the case where extra assembly levels are required. For the sake of simplicity, in this work, we assume that the assembled subsets obtained from step 2 will not be further connected with additional subsets. If the size of the CDOFs is still too large and a further reduction is desired, a modal truncation for the CDOFs can be performed as for the system-level reduction in Sec. III.A.

To apply the multilevel interface reduction for an arbitrary system, we start with the stage where all the substructures are reduced with the CB method, as discussed in Sec. II.A. The substructures within the  $i$ th subset  $\Gamma_i$  are then assembled together in the primal way by defining a unique set of interface DOFs within the subset. The assembly procedure is identical to the primal assembly introduced in Sec. II.B, and it will not be repeated here. The reduced EOMs are analogous to Eq. (6) and are written here for the  $i$ th subset  $\Gamma_i$  as

$$\underbrace{\begin{bmatrix} M_{\Gamma_i}^{BB} & M_{\Gamma_i}^{BI} \\ M_{\Gamma_i}^{IB} & I_{\Gamma_i}^{II} \end{bmatrix}}_{M_{\Gamma_i}} \begin{bmatrix} \ddot{\mathbf{q}}_{\Gamma_i}^B \\ \ddot{\boldsymbol{\eta}}_{\Gamma_i}^I \end{bmatrix} + \underbrace{\begin{bmatrix} K_{\Gamma_i}^{BB} & \mathbf{0} \\ \mathbf{0} & \omega_{\Gamma_i}^2 \end{bmatrix}}_{K_{\Gamma_i}} \begin{bmatrix} \mathbf{q}_{\Gamma_i}^B \\ \boldsymbol{\eta}_{\Gamma_i}^I \end{bmatrix} = \underbrace{\begin{bmatrix} \mathbf{g}_{\Gamma_i}^B \\ \mathbf{g}_{\Gamma_i}^I \end{bmatrix}}_{\mathbf{g}_{\Gamma_i}} + \begin{bmatrix} \mathbf{p}_{\Gamma_i}^B \\ \mathbf{0} \end{bmatrix}, \quad i = 1, 2, \dots, Z \quad (15)$$

where the connecting force imposed by the neighboring subset is indicated by  $\mathbf{p}_{\Gamma_i}^B$  to satisfy the force equilibrium, and  $Z$  is the number of subsets for the entire system. For the  $i$ th subset,  $\mathbf{q}_{\Gamma_i}^B$  is a unique set of the interface DOFs, and  $\boldsymbol{\eta}_{\Gamma_i}^I$  is the internal DOFs. The formulation of all partitioned mass matrices  $M_{\Gamma_i}$ , stiffness matrices  $K_{\Gamma_i}$ , and external load vectors  $\mathbf{g}_{\Gamma_i}$  can be derived as described in Sec. II.B.

As mentioned in step 2, the interface DOFs  $\mathbf{q}_{\Gamma_i}^B$  of the subset  $\Gamma_i$  are partitioned into two sets (i.e., CDOFs  $\mathbf{q}_{\Gamma_i}^C$  and NDOFs  $\mathbf{q}_{\Gamma_i}^N$ ) by expressing that

$$\mathbf{q}_{\Gamma_i}^B = \text{col}(\mathbf{q}_{\Gamma_i}^C, \mathbf{q}_{\Gamma_i}^N)$$

With this notation, Eq. (15) can be rewritten for an arbitrary structure with  $Z$  subsets in a generalized fashion:

$$\underbrace{\begin{bmatrix} M_{\Gamma_i}^{CC} & M_{\Gamma_i}^{CN} & M_{\Gamma_i}^{CI} \\ M_{\Gamma_i}^{NC} & M_{\Gamma_i}^{NN} & M_{\Gamma_i}^{NI} \\ M_{\Gamma_i}^{IC} & M_{\Gamma_i}^{IN} & I_{\Gamma_i}^{II} \end{bmatrix}}_{M_{\Gamma_i}} \begin{bmatrix} \ddot{\mathbf{q}}_{\Gamma_i}^C \\ \ddot{\mathbf{q}}_{\Gamma_i}^N \\ \ddot{\boldsymbol{\eta}}_{\Gamma_i}^I \end{bmatrix} + \underbrace{\begin{bmatrix} K_{\Gamma_i}^{CC} & K_{\Gamma_i}^{CN} & \mathbf{0} \\ K_{\Gamma_i}^{NC} & K_{\Gamma_i}^{NN} & \mathbf{0} \\ \mathbf{0} & \mathbf{0} & \omega_{\Gamma_i}^2 \end{bmatrix}}_{K_{\Gamma_i}} \begin{bmatrix} \mathbf{q}_{\Gamma_i}^C \\ \mathbf{q}_{\Gamma_i}^N \\ \boldsymbol{\eta}_{\Gamma_i}^I \end{bmatrix} = \underbrace{\begin{bmatrix} \mathbf{g}_{\Gamma_i}^C \\ \mathbf{g}_{\Gamma_i}^N \\ \mathbf{g}_{\Gamma_i}^I \end{bmatrix}}_{\mathbf{g}_{\Gamma_i}} + \begin{bmatrix} \mathbf{p}_{\Gamma_i}^C \\ \mathbf{0} \\ \mathbf{0} \end{bmatrix} \quad (16)$$

To further reduce the size of system matrices in Eq. (16), a secondary CB projection is applied at each subset independently. As mentioned in step 2, we propose two ROMs for the multilevel interface reduction techniques. To assemble the neighboring subsets in a fully compatible way, CDOFs  $\mathbf{q}_{\Gamma_i}^C$  are treated as the interface for the CB reduction, and thus are not reduced in both methods.

For ML1-ROM, a secondary CB reduction is performed only for the interface DOFs (CDOFs  $\mathbf{q}_{\Gamma_i}^C$  and NDOFs  $\mathbf{q}_{\Gamma_i}^N$ ) by stating

$$\begin{bmatrix} \mathbf{q}_{\Gamma_i}^C \\ \mathbf{q}_{\Gamma_i}^N \\ \boldsymbol{\eta}_{\Gamma_i}^I \end{bmatrix} = \begin{bmatrix} I & \mathbf{0} & \mathbf{0} \\ \tilde{\Psi}_{\Gamma_i}^{NC} & \tilde{\Phi}_{\Gamma_i}^{NN} & \mathbf{0} \\ \mathbf{0} & \mathbf{0} & I \end{bmatrix} \begin{bmatrix} \mathbf{q}_{\Gamma_i}^C \\ \boldsymbol{\eta}_{\Gamma_i}^N \\ \boldsymbol{\eta}_{\Gamma_i}^I \end{bmatrix} \quad (17)$$

where the modes  $\tilde{\Psi}_{\Gamma_i}^{NC}$  are denoted here as the interface-level constraint modes (ILCMs), and the modes  $\tilde{\Phi}_{\Gamma_i}^{NN}$  are called the interface-level internal vibration modes (ILIVMs). The ILCMs  $\tilde{\Psi}_{\Gamma_i}^{NC}$  and ILIVMs  $\tilde{\Phi}_{\Gamma_i}^{NN}$  are calculated as

$$\tilde{\Psi}_{\Gamma_i}^{NC} = -\left(K_{\Gamma_i}^{NN}\right)^{-1} K_{\Gamma_i}^{NC} \quad \text{and} \quad K_{\Gamma_i}^{NN} \tilde{\Phi}_{\Gamma_i}^{NN} - M_{\Gamma_i}^{NN} \tilde{\Phi}_{\Gamma_i}^{NN} \boldsymbol{\zeta}_{\Gamma_i}^2 = \mathbf{0} \quad (18)$$

The ILIVMs  $\tilde{\Phi}_{\Gamma_i}^{NN}$  are truncated based on the frequency range of interest, and  $\boldsymbol{\zeta}_{\Gamma_i}^2$  is the corresponding diagonal eigenfrequency matrix. It is worth noticing that the size of the eigenvalue problems [Eq. (18)] is much smaller than that of the system-level counterpart [Eq. (8)], and therefore computationally less demanding.

For ML2-ROM, a secondary CB reduction is performed for all DOFs within the  $i$ th subset; the NDOFs  $\mathbf{q}_{\Gamma_i}^N$  and IDOFs  $\boldsymbol{\eta}_{\Gamma_i}^I$  are merged together and further reduced during the modal truncation. The CB reduction can be expressed as

$$\begin{bmatrix} \mathbf{q}_{\Gamma_i}^C \\ \mathbf{q}_{\Gamma_i}^N \\ \boldsymbol{\eta}_{\Gamma_i}^I \end{bmatrix} = \begin{bmatrix} I & \mathbf{0} \\ \tilde{\Psi}_{\Gamma_i}^{NC} & \tilde{\Phi}_{\Gamma_i}^{NM} \\ \mathbf{0} & \tilde{\Phi}_{\Gamma_i}^{IM} \end{bmatrix} \begin{bmatrix} \mathbf{q}_{\Gamma_i}^C \\ \boldsymbol{\eta}_{\Gamma_i}^M \end{bmatrix} \quad (19)$$

where  $\tilde{\Phi}_{\Gamma_i}^{NM}$  and  $\tilde{\Phi}_{\Gamma_i}^{IM}$  are the rows of merged internal vibration modes (MIVMs)  $\tilde{\Phi}_{\Gamma_i}^M$  corresponding to NDOFs and IDOFs, respectively. To calculate the MIVMs, the eigenvalue analysis is applied to the ROM in Eq. (16), when CDOFs  $\mathbf{q}_{\Gamma_i}^C$  are fixed, as

$$\begin{bmatrix} K_{\Gamma_i}^{NN} & \mathbf{0} \\ \mathbf{0} & \omega_{\Gamma_i}^2 \end{bmatrix} \begin{bmatrix} \tilde{\Phi}_{\Gamma_i}^{NM} \\ \tilde{\Phi}_{\Gamma_i}^{IM} \end{bmatrix} - \begin{bmatrix} M_{\Gamma_i}^{NN} & M_{\Gamma_i}^{NI} \\ M_{\Gamma_i}^{IN} & I_{\Gamma_i}^{II} \end{bmatrix} \begin{bmatrix} \tilde{\Phi}_{\Gamma_i}^{NM} \\ \tilde{\Phi}_{\Gamma_i}^{IM} \end{bmatrix} \boldsymbol{\tau}_{\Gamma_i}^2 = \mathbf{0} \quad (20)$$

where the MIVMs  $\tilde{\Phi}_{\Gamma_i}^M$  are truncated, as before, based on the frequency range of interest; and  $\boldsymbol{\tau}_{\Gamma_i}^2$  is the corresponding diagonal eigenfrequency matrix.

It should be noticed here that the computational cost of the eigenvalue solution in Eq. (20) is slightly more expensive when compared to its counterpart in Eq. (18) because the IDOFs  $\boldsymbol{\eta}_{\Gamma_i}^I$  are also included. However, the size of  $\boldsymbol{\eta}_{\Gamma_i}^I$  will not be large if assuming that the internal DOFs of each subsystem have already been significantly reduced during the CB projection as discussed in Sec. II.A. Therefore, the computational cost of Eq. (20) will still be small when compared to its counterpart [Eq. (8)] in the SL-ROM.

By substituting the interface CB reduction for the ML1-ROM [Eq. (17)] and ML2-ROM [Eq. (19)] into Eq. (16) and projecting, we obtain

$$\begin{aligned} & \begin{bmatrix} \tilde{M}_{\Gamma_i}^{CC} & \tilde{M}_{\Gamma_i}^{CN} & \tilde{M}_{\Gamma_i}^{CI} \\ \tilde{M}_{\Gamma_i}^{NC} & I_{\Gamma_i}^{NN} & \tilde{M}_{\Gamma_i}^{NI} \\ \tilde{M}_{\Gamma_i}^{LC} & \tilde{M}_{\Gamma_i}^{LN} & I_{\Gamma_i}^{LL} \end{bmatrix} \begin{bmatrix} \ddot{\mathbf{q}}_{\Gamma_i}^C \\ \ddot{\boldsymbol{\eta}}_{\Gamma_i}^N \\ \ddot{\boldsymbol{\eta}}_{\Gamma_i}^L \end{bmatrix} + \begin{bmatrix} \tilde{K}_{\Gamma_i}^{CC} & \mathbf{0} & \mathbf{0} \\ \mathbf{0} & \boldsymbol{\varsigma}_{\Gamma_i}^2 & \mathbf{0} \\ \mathbf{0} & \mathbf{0} & \omega_{\Gamma_i}^2 \end{bmatrix} \begin{bmatrix} \mathbf{q}_{\Gamma_i}^C \\ \boldsymbol{\eta}_{\Gamma_i}^N \\ \boldsymbol{\eta}_{\Gamma_i}^L \end{bmatrix} \\ &= \begin{bmatrix} \tilde{\mathbf{g}}_{\Gamma_i}^C \\ \tilde{\mathbf{g}}_{\Gamma_i}^N \\ \tilde{\mathbf{g}}_{\Gamma_i}^L \end{bmatrix} + \begin{bmatrix} \mathbf{p}_{\Gamma_i}^C \\ \mathbf{0} \\ \mathbf{0} \end{bmatrix} \quad \text{for ML 1-ROM} \end{aligned} \quad (21)$$

and

$$\begin{aligned} & \begin{bmatrix} \tilde{M}_{\Gamma_i}^{CC} & \tilde{M}_{\Gamma_i}^{CM} \\ \tilde{M}_{\Gamma_i}^{MC} & I_{\Gamma_i}^{MM} \end{bmatrix} \begin{bmatrix} \ddot{\mathbf{q}}_{\Gamma_i}^C \\ \ddot{\boldsymbol{\eta}}_{\Gamma_i}^M \end{bmatrix} + \begin{bmatrix} \tilde{K}_{\Gamma_i}^{CC} & \mathbf{0} \\ \mathbf{0} & \boldsymbol{\tau}_{\Gamma_i}^2 \end{bmatrix} \begin{bmatrix} \mathbf{q}_{\Gamma_i}^C \\ \boldsymbol{\eta}_{\Gamma_i}^M \end{bmatrix} \\ &= \begin{bmatrix} \tilde{\mathbf{g}}_{\Gamma_i}^C \\ \tilde{\mathbf{g}}_{\Gamma_i}^M \end{bmatrix} + \begin{bmatrix} \mathbf{p}_{\Gamma_i}^C \\ \mathbf{0} \end{bmatrix} \quad \text{for ML 2-ROM} \end{aligned} \quad (22)$$

where the formulation of all partitioned matrices and vectors can be easily derived from the Galerkin projection, and it will not be discussed here.

Once all the reduced subsets are constructed, we need to assemble them in a primal manner by choosing a unique set of CDOFs, which is denoted here as  $\mathbf{q}_\Gamma^C$ . The assembly procedure is identical to the primal assembly introduced in Sec. II.B. The reduced EOMs for the entire system are analogous to Eq. (6) and are directly written here as

$$\begin{aligned} & \begin{bmatrix} \tilde{M}_\Gamma^{CC} & \tilde{M}_\Gamma^{CN} & \tilde{M}_\Gamma^{CI} \\ \tilde{M}_\Gamma^{NC} & I_\Gamma^{NN} & \tilde{M}_\Gamma^{NI} \\ \tilde{M}_\Gamma^{LC} & \tilde{M}_\Gamma^{LN} & I_{CB}^{LL} \end{bmatrix} \begin{bmatrix} \ddot{\mathbf{q}}_\Gamma^C \\ \ddot{\boldsymbol{\eta}}_\Gamma^N \\ \ddot{\boldsymbol{\eta}}_{CB}^L \end{bmatrix} + \begin{bmatrix} \tilde{K}_\Gamma^{CC} & \mathbf{0} & \mathbf{0} \\ \mathbf{0} & \boldsymbol{\varsigma}^2 & \mathbf{0} \\ \mathbf{0} & \mathbf{0} & \omega_{CB}^2 \end{bmatrix} \begin{bmatrix} \mathbf{q}_\Gamma^C \\ \boldsymbol{\eta}_\Gamma^N \\ \boldsymbol{\eta}_{CB}^L \end{bmatrix} \\ &= \begin{bmatrix} \tilde{\mathbf{g}}_\Gamma^C \\ \tilde{\mathbf{g}}_\Gamma^N \\ \tilde{\mathbf{g}}_{CB}^L \end{bmatrix} \quad \text{for ML 1-ROM} \end{aligned} \quad (23)$$

and

$$\begin{aligned} & \begin{bmatrix} \tilde{M}_\Gamma^{CC} & \tilde{M}_\Gamma^{CM} \\ \tilde{M}_\Gamma^{MC} & I_\Gamma^{MM} \end{bmatrix} \begin{bmatrix} \ddot{\mathbf{q}}_\Gamma^C \\ \ddot{\boldsymbol{\eta}}_\Gamma^M \end{bmatrix} + \begin{bmatrix} \tilde{K}_\Gamma^{CC} & \mathbf{0} \\ \mathbf{0} & \boldsymbol{\tau}^2 \end{bmatrix} \begin{bmatrix} \mathbf{q}_\Gamma^C \\ \boldsymbol{\eta}_\Gamma^M \end{bmatrix} \\ &= \begin{bmatrix} \tilde{\mathbf{g}}_\Gamma^C \\ \tilde{\mathbf{g}}_\Gamma^M \end{bmatrix} \quad \text{for ML 2-ROM} \end{aligned} \quad (24)$$

where

$$\boldsymbol{\varsigma}^2 = \text{diag}(\boldsymbol{\varsigma}_{\Gamma_1}^2, \dots, \boldsymbol{\varsigma}_{\Gamma_z}^2)$$

$$\boldsymbol{\tau}^2 = \text{diag}(\boldsymbol{\tau}_{\Gamma_1}^2, \dots, \boldsymbol{\tau}_{\Gamma_z}^2)$$

$$\boldsymbol{\eta}_\Gamma^N = \text{col}(\boldsymbol{\eta}_{\Gamma_1}^N, \dots, \boldsymbol{\eta}_{\Gamma_z}^N)$$

and

$$\boldsymbol{\eta}_\Gamma^M = \text{col}(\boldsymbol{\eta}_{\Gamma_1}^M, \dots, \boldsymbol{\eta}_{\Gamma_z}^M)$$

The formulation of all the partitioned mass and stiffness matrices in Eqs. (23) and (24) can be derived as described in [31], and they will not be discussed here.

If a further reduction of the CDOFs  $\mathbf{q}_\Gamma^C$  is still desired, we can apply the system-level interface reduction technique as discussed in Sec. III.A. By fixing  $\boldsymbol{\eta}_{\Gamma_1}^N$  and  $\boldsymbol{\eta}_{CB}^L$  in Eq. (23) or fixing  $\boldsymbol{\eta}_\Gamma^M$  in Eq. (24),

we get

$$\tilde{M}_\Gamma^{CC} \ddot{\mathbf{q}}_\Gamma^C + \tilde{K}_\Gamma^{CC} \mathbf{q}_\Gamma^C = \tilde{\mathbf{g}}_\Gamma^C \quad (25)$$

where

$$\tilde{M}_\Gamma^{CC} \in \mathbb{R}^{n_\Gamma^C \times n_\Gamma^C}, \quad \tilde{K}_\Gamma^{CC} \in \mathbb{R}^{n_\Gamma^C \times n_\Gamma^C}$$

are the mass and stiffness matrices when all DOFs are statically condensed to the CDOFs, and  $n_\Gamma^C$  is the size of vector  $\mathbf{q}_\Gamma^C$ . Then, the motion of  $\mathbf{q}_\Gamma^C$  is approximated by performing a modal truncation as

$$\mathbf{q}_\Gamma^C = \tilde{\Phi}_\Gamma^{CC} \boldsymbol{\eta}_\Gamma^C, \quad \text{with} \quad (\tilde{K}_\Gamma^{CC} - v_j^2 \tilde{M}_\Gamma^{CC}) \tilde{\boldsymbol{\phi}}_{j,\Gamma}^{CC} = \mathbf{0}, \quad j = 1, \dots, n_\Gamma^C \quad (26)$$

where the interface-level characteristic constraint (ILCC) modes

$$\tilde{\Phi}_\Gamma^{CC} = [\tilde{\boldsymbol{\phi}}_{1,\Gamma}^{CC}, \dots, \tilde{\boldsymbol{\phi}}_{m_\Gamma^C,\Gamma}^{CC}]$$

are a truncated set of the eigenvectors, with  $m_\Gamma^C \ll n_\Gamma^C$ . The corresponding eigenvalues can be rewritten in a diagonal matrix form as  $\mathbf{v}^2 = \text{diag}(v_1^2, \dots, v_{m_\Gamma^C}^2)$ .

Substitution of the interface reduction [Eq. (26)] to Eqs. (23) and (24) via a Galerkin projection then gives the final reduced EOMs for the ML1-ROM as

$$\begin{aligned} & \underbrace{\begin{bmatrix} I_\Gamma^{CC} & (\tilde{\Phi}_\Gamma^{CC})^T \tilde{M}_\Gamma^{CN} & (\tilde{\Phi}_\Gamma^{CC})^T \tilde{M}_\Gamma^{CI} \\ \tilde{M}_\Gamma^{NC} \tilde{\Phi}_\Gamma^{CC} & I_\Gamma^{NN} & \tilde{M}_\Gamma^{NI} \\ \tilde{M}_\Gamma^{LC} \tilde{\Phi}_\Gamma^{CC} & \tilde{M}_\Gamma^{LN} & I_{CB}^{LL} \end{bmatrix}}_{\tilde{M}_{M\Gamma 1}} \begin{bmatrix} \ddot{\boldsymbol{\eta}}_\Gamma^C \\ \ddot{\boldsymbol{\eta}}_\Gamma^N \\ \ddot{\boldsymbol{\eta}}_{CB}^L \end{bmatrix} \\ &+ \underbrace{\begin{bmatrix} \mathbf{v}^2 & \mathbf{0} & \mathbf{0} \\ \mathbf{0} & \boldsymbol{\varsigma}^2 & \mathbf{0} \\ \mathbf{0} & \mathbf{0} & \omega_{CB}^2 \end{bmatrix}}_{\tilde{K}_{M\Gamma 1}} \begin{bmatrix} \boldsymbol{\eta}_\Gamma^C \\ \boldsymbol{\eta}_\Gamma^N \\ \boldsymbol{\eta}_{CB}^L \end{bmatrix} = \underbrace{\begin{bmatrix} (\tilde{\Phi}_\Gamma^{CC})^T \tilde{\mathbf{g}}_\Gamma^C \\ \tilde{\mathbf{g}}_\Gamma^N \\ \tilde{\mathbf{g}}_{CB}^L \end{bmatrix}}_{\tilde{\mathbf{g}}_{M\Gamma 1}} \end{aligned} \quad (27)$$

and for the ML2-ROM as

$$\begin{aligned} & \underbrace{\begin{bmatrix} I_\Gamma^{CC} & (\tilde{\Phi}_\Gamma^{CC})^T \tilde{M}_\Gamma^{CM} \\ \tilde{M}_\Gamma^{MC} \tilde{\Phi}_\Gamma^{CC} & I_\Gamma^{MM} \end{bmatrix}}_{\tilde{M}_{M\Gamma 2}} \begin{bmatrix} \ddot{\boldsymbol{\eta}}_\Gamma^C \\ \ddot{\boldsymbol{\eta}}_\Gamma^M \end{bmatrix} + \underbrace{\begin{bmatrix} \mathbf{v}^2 & \mathbf{0} \\ \mathbf{0} & \boldsymbol{\tau}^2 \end{bmatrix}}_{\tilde{K}_{M\Gamma 2}} \begin{bmatrix} \boldsymbol{\eta}_\Gamma^C \\ \boldsymbol{\eta}_\Gamma^M \end{bmatrix} \\ &= \underbrace{\begin{bmatrix} (\tilde{\Phi}_\Gamma^{CC})^T \tilde{\mathbf{g}}_\Gamma^C \\ \tilde{\mathbf{g}}_\Gamma^M \end{bmatrix}}_{\tilde{\mathbf{g}}_{M\Gamma 2}} \end{aligned} \quad (28)$$

As can be noticed, the reduced stiffness matrices in both Eqs. (27) and (28) are both fully diagonal, as is the case in Eq. (9) when adopting the system-level interface reduction. Here, we stress that the effort in obtaining Eqs. (27) and (28) is lower than its counterpart in the system-level approach discussed in Sec. III.A.

For illustration, we take the  $\Gamma$ -shaped model in Fig. 4 as an example. The CB-reduced subsystems are grouped into two local subsets: subset  $\Gamma_1$ , comprising substructures  $S_1$  and  $S_2$ ; and subset  $\Gamma_2$ , comprising substructures  $S_3$  and  $S_4$ . The interface DOFs of the  $\Gamma$ -shaped model are here partitioned into three components as  $B_1$ ,  $B_2$ , and  $B_3$ . In this model, the interface  $B_2$  acts as the boundary component of the interface DOFs (CDOFs), which connects the subsets  $\Gamma_1$  and  $\Gamma_2$ . We show the different reduction bases of these two multilevel interface reduction techniques in Fig. 4. For both the ML1-ROM and ML2-ROM, we subdivide the interface reduction

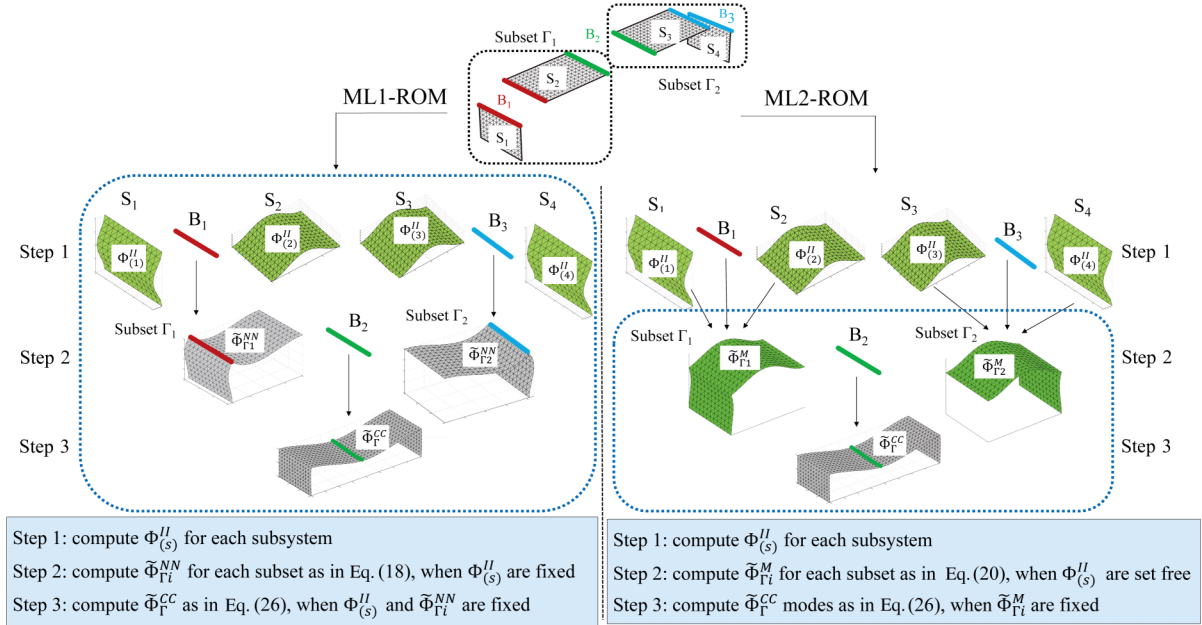


**Fig. 4** Illustration of the two multilevel interface reduction techniques for the  $\pi$ -shaped model.

procedure into three steps. The first step, as discussed, is CB reduction at the subsystem level. In the ML1-ROM, the gray mesh indicates that the internal DOFs are condensed at step 2. All the truncated eigenvectors (i.e., IVMs and ILVMs) from step 1 to step 2 are kept in the final reduction basis. In the ML2-ROM, the IVMs of each substructure at step 1 are then discarded because the merged vibration modes of the assembled subset are used to reproduce the dynamics of the subset itself. With the same frequency cutoff criterion, the ML2-ROM will generally result in a reduction basis with smaller size when compared to the ML1-ROM.

In the next section, a detailed analysis of the computational cost associated to the multilevel interface reduction will be given. We show the computational advantages of the proposed methods as compared to the system-level and local-level approaches.

## V. Computational Complexity

We estimate here the computational cost associated to the proposed multilevel interface reduction and compare it to the system- and local-level approaches. We start with the given CB basis in Eq. (3) and reduced EOMs in Eq. (6), which are the foundation for all the interface reduction methods.

For the SL-ROM, the solution of eigenvalue problems for the interface partition of the assembled CB matrices in Eq. (8) is the most involved operation. For the dense matrices  $\tilde{K}_{CB}^{BB}$  and  $\tilde{M}_{CB}^{BB}$ , the solution of the eigenvalue problem takes  $\mathcal{O}[(n_{CB}^B)^3]$  flops using QR and QZ methods [35], where  $n_{CB}^B$  is the number of a unique set of all interface DOFs.

For the LL-ROM, the secondary eigenvalue analysis in Eq. (11) is performed for the interface DOFs of each subsystem locally. Take the

$s$ th subsystem, for instance; it takes  $\mathcal{O}[(n_{(s)}^B)^3]$  flops for the eigenvalue analysis for the dense matrices  $\tilde{K}_{(s)}^{BB}$  and  $\tilde{M}_{(s)}^{BB}$ , where  $n_{(s)}^B$  is the number of interface DOFs for the  $s$ th substructure. To prevent ill conditioning, in Eq. (12), a singular value analysis is used to reshape the LCC modes  $\tilde{\Phi}_{LC}^{B_i}$  for each interface set  $B_i$ , which will take [36]  $\mathcal{O}[n^{B_i} \times (m^{B_i})^2]$  flops where  $n^{B_i}$  is the number of DOFs at interface  $B_i$ , and  $m^{B_i}$  is the number of truncated LCC modes from substructures connecting through interface  $B_i$ .

For the ML1-ROM, solving the eigenvalue problem in Eq. (18) of the interface-level subset  $\Gamma_i$  takes  $\mathcal{O}[(n_{\Gamma_i}^N)^3]$  flops where  $n_{\Gamma_i}^N$  is the size of vector  $\mathbf{q}_{\Gamma_i}^N$  for the subset  $\Gamma_i$ . For the ML2-ROM, solving the eigenvalue problem in Eq. (20) takes  $\mathcal{O}[(n_{\Gamma_i}^N + m_{\Gamma_i}^I)^3]$  flops where  $m_{\Gamma_i}^I$  is the number of IVMs of the subsystems within the subset  $\Gamma_i$ . In general, the IVMs in each subsystem have been efficiently truncated so that  $m_{\Gamma_i}^I \ll n_{\Gamma_i}^N$ . Therefore, the extra computational cost associated to the ML2-ROM when compared to the ML1-ROM will be only marginal. The solution of interface-level CMs in Eq. (18) for subset  $\Gamma_i$  is the same for both the ML1-ROM and ML2-ROM. It requires the factorization of the dense matrix  $\tilde{K}_{\Gamma_i}^{NN}$ , which is also computationally expensive. In fact, the complexity of the factorization of a dense  $n_{\Gamma_i}^N \times n_{\Gamma_i}^N$  matrix is given by  $\mathcal{O}[(n_{\Gamma_i}^N)^{2.38}]$  flops, see [37]. If a further reduction of the CDOFs  $\mathbf{q}_{\Gamma_i}^C$  is desired, the eigenvalue analysis in Eq. (26) will take an extra  $\mathcal{O}[(n_{\Gamma_i}^C)^3]$  operations where  $n_{\Gamma_i}^C$  is the size of vector  $\mathbf{q}_{\Gamma_i}^C$ .

All the estimated costs are summarized in Table 1. It shows that the computational cost of the different techniques mainly depends on the number of interface DOFs involved in the reduction procedures.

**Table 1** Computational cost estimation of the most expensive operations of different interface reduction techniques

Method	Significant operations		
SL-ROM	Eigenvalue analysis in Eq. (8) $\mathcal{O}[(n_{CB}^B)^3]$		
LL-ROM	Eigenvalue analysis in Eq. (11) $\mathcal{O}[(n_{(s)}^B)^3]$	Singular value decomposition in Eq. (12) $\mathcal{O}[n^{B_i} \times (m^{B_i})^2]$	
ML1-ROM	Eigenvalue analysis in Eq. (18) $\mathcal{O}[(n_{\Gamma_i}^N)^3]$	Matrix factorization in Eq. (18) $\mathcal{O}[(n_{\Gamma_i}^N)^{2.38}]$	Eigenvalue analysis in Eq. (26) $\mathcal{O}[(n_{\Gamma_i}^C)^3]$
ML2-ROM	Eigenvalue analysis in Eq. (20) $\mathcal{O}[(n_{\Gamma_i}^N + m_{\Gamma_i}^I)^3]$	Matrix factorization in Eq. (18) $\mathcal{O}[(n_{\Gamma_i}^N)^{2.38}]$	Eigenvalue analysis in Eq. (26) $\mathcal{O}[(n_{\Gamma_i}^C)^3]$

As opposed to the system-level interface reduction, the local-level and multilevel methods can be applied for each substructure/subset in parallel. For clarity, we labeled the parallelizable operations for each substructure/subset with the symbol  $\parallel$  in Table 1. Each of these models are of significantly smaller size as compared to the full model. Therefore, the computational cost for the LL-ROM, ML1-ROM, and ML2-ROM only depends on the maximum cost associated to the largest subcomponent/subset. Given a system with a large number of substructures and interface sets, it always holds that

$$n_{CB}^B > \max(n_{(s)}^B), n_{CB}^B > \max(n^{B_i}), \text{ with } s = 1, \dots, H; i = 1, \dots, V \quad (29)$$

when the SL-ROM and LL-ROM are compared; and

$$n_{CB}^B > n_{\Gamma}^C, n_{CB}^B > \max(n_{\Gamma_j}^N), n_{CB}^B > \max(n_{\Gamma_j}^N + m_{\Gamma_j}^I), \text{ with } j = 1, \dots, Z \quad (30)$$

when we compared the performances between the SL-ROM and ML1-ROM or ML2-ROM.

Equations (29) and (30) indicate that the number of interface DOFs for the entire system is much larger than the one of a single substructure/subset. This highlights the potential computational savings of performing the local-level and multilevel interface reduction techniques with respect to the system-level interface reduction when parallel computation is performed for each substructure/subset with a much smaller size.

In this work, we also compare the computational efficiency of different interface reduction methods when a transient analysis is performed on the so obtained ROMs. The implicit Newmark method is adopted for the time integration, with parameters  $\alpha = 1/2$  and  $\beta = 1/4$ . The detailed procedure of the Newmark method can be found in [38]. The calculation of the modal amplitude increment  $\Delta \eta$  at each time step, which is the most time-consuming operation, is given by

$$\Delta \eta = \mathcal{K}^{-1} r, \quad \text{with } \mathcal{K} = M + \beta \Delta t^2 K + \alpha \Delta t C \quad (31)$$

where  $\mathcal{K}$  is the dynamic stiffness matrix, which can be computed based on the reduced stiffness and mass matrices in different interface reduction basis. The Rayleigh damping is adopted, and the coefficients are chosen to match a modal damping of 0.02 for the first two modes (see [39] for details). The Cholesky factorization of the dynamic stiffness matrices  $\mathcal{K}$  is applied before the time integration. The computational cost of the time integration is mainly determined by the size of the ROMs, as shown in the following section.

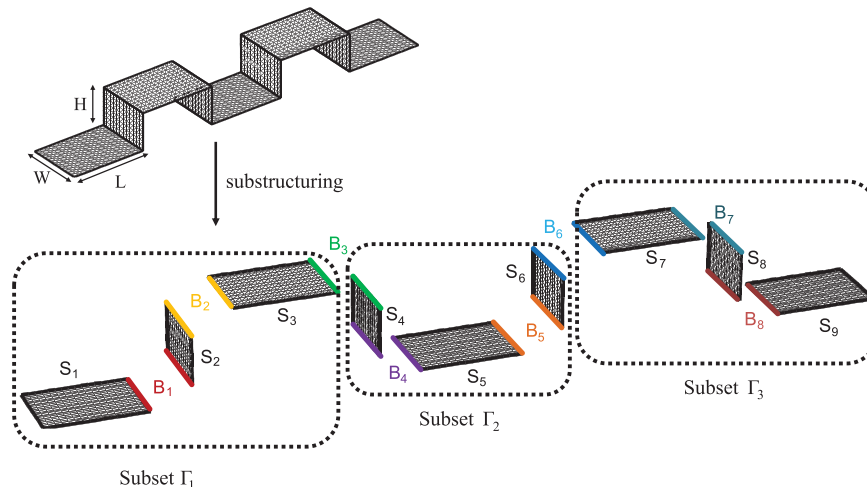


Fig. 5 Illustration of the double- $\pi$ -shaped FE model.

## VI. Numerical Examples

To assess the accuracy of the different methods, we compare the eigenfrequencies and eigenmodes obtained by using different ROMs for two numerical examples. The linear dynamic response is further investigated in Sec. VI.B. In particular, we refer to the full model (i.e., without reduction) as Full, the CB-reduced model (without interface reduction) as CB-ROM; the system-level, local-level, and two multilevel reduced models are denoted by SL-ROM, LL-ROM, ML1-ROM, and ML2-ROM, respectively.

### A. Double- $\pi$ Shaped FE Model

A double- $\pi$ -shaped FE model that consists of nine subcomponents is considered here. The geometry of the structure and material properties are shown in Fig. 5. The length is  $L = 0.4064$  m, the width is  $W = 0.3048$  m, the height is  $H = 0.2030$  m, and the thickness is  $t = 0.003175$  m. The Young modulus is  $E = 7.31 \times 10^{10}$  Pa, the Poisson's ratio is  $\nu = 0.33$ , and the density is  $\rho = 2795.7$  kg  $\cdot$  m $^{-3}$ . The structure has been divided into nine substructures ( $S_1$  to  $S_9$ ), which are connected through eight interface sets ( $B_1$  to  $B_8$ ). For the multilevel interface reduction, the interface sets are further split into three subsets ( $\Gamma_1$  to  $\Gamma_3$ ). The structure is meshed with triangular flat shell elements with six DOFs per node. The resulting FE model has a total of 8814 DOFs, including  $n_{CB}^B = 624$  interface DOFs and  $n_G^I = 8190$  internal DOFs, with

$$n_G^I = \sum_{s=1}^9 n_{(s)}^I$$

The system has been clamped at two ends.

We are interested in the first 30 eigenfrequencies and eigenmodes of the system. For the CB-ROM, the first  $m_{(s)}^I = 10$  IVMs  $\Phi_{(s)}^I$  are selected for each substructure; thus, the number of internal DOFs is reduced from  $n_G^I = 8190$  to  $m_{CB}^I = 90$  DOFs, whereas all the  $n_{CB}^B = 624$  interface DOFs are retained without reduction. The 624 CMs are replaced with the first  $m_{SC}^B = 80$  SCC modes  $\tilde{\Phi}_{SC}^B$  by applying further system-level interface reduction methods for the SL-ROM. The LL-ROM is constructed by replacing the CMs in each substructure with the first  $m_{(s)}^B = 12$  LCC modes  $\tilde{\Phi}_{LL,(s)}^B$ . By using a SVD for each interface that is set to guard against ill conditioning and by using the threshold discussed previously, finally, 145 interface modes are retained in the reduction basis. The ML1-ROM is formed by  $m_{\Gamma_1}^N = 20$  interface-level IVMs  $\tilde{\Phi}_{\Gamma_1}^{NN}$  for each subset ( $\Gamma_1$  to  $\Gamma_3$ ) together with  $m_{\Gamma_1}^C = 20$  ILCC modes  $\tilde{\Phi}_{\Gamma_1}^{CC}$ . The ML2-ROM is formed by the first 50 MIVMs  $\tilde{\Phi}_{\Gamma_1}^M$  for each subset and  $m_{\Gamma_1}^C = 20$  interface-level characteristic constraint (CC) modes  $\tilde{\Phi}_{\Gamma_1}^{CC}$ . We determine the number of kept modes for different interface reduction methods in such a way that the SL-ROM, ML1-ROM, and ML2-ROM all result

**Table 2** Number of modal coordinates of the double- $\Gamma$ -shaped model for different ROMs

ROMs	Number of modal coordinates		Total DOFs	
CB-ROM	$q_{CB}^B$ 624	$\eta_{CB}^I$ 90	$\text{col}(q_{CB}^B, \eta_{CB}^I)$ 714	
SL-ROM	$\eta_{SL}^B$ 80	$\eta_{CB}^I$ 90	$\text{col}(\eta_{SL}^B, \eta_{CB}^I)$ 170	
LL-ROM	$\eta_{LL}^B$ 145	$\eta_{CB}^I$ 90	$\text{col}(\eta_{LL}^B, \eta_{CB}^I)$ 235	
ML1-ROM	$\eta_{\Gamma}^C$ 20	$\eta_{\Gamma}^N$ 60	$\eta_{CB}^I$ 90	$\text{col}(\eta_{\Gamma}^C, \eta_{\Gamma}^N, \eta_{CB}^I)$ 170
ML2-ROM	$\eta_{\Gamma}^C$ 20	$\eta_{\Gamma}^M$ 150		$\text{col}(\eta_{\Gamma}^C, \eta_{\Gamma}^M)$ 170

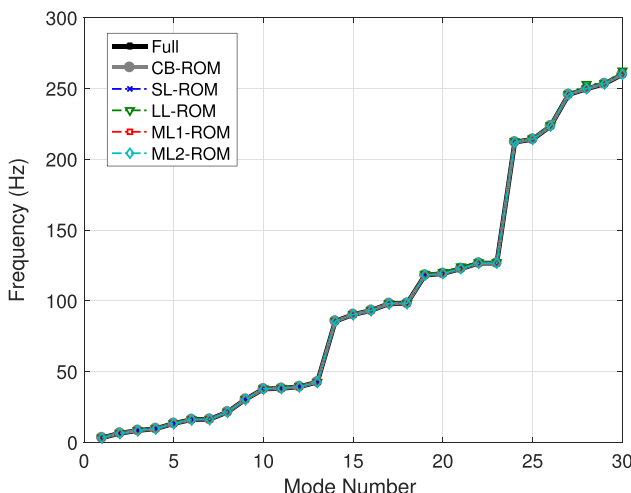
in 170 modes in the final reduction basis. For illustration, the number of DOFs for different ROMs is summarized in Table 2.

The first 30 eigenfrequencies and the corresponding relative error with respect to the full model are shown in Fig. 6. Note that any interface ROM will not be more accurate than its parent CB-ROM. As can be seen in Fig. 6b, the eigenfrequency error for all the considered ROMs is below 1% for the first 30 frequencies. Except for the LL-ROM, the other considered ROMs keep the error within 0.1%. The SL-ROM, ML1-ROM, and ML2-ROM lead to an accuracy that is orders of magnitude better in the low-frequency range when compared to the LL-ROM, although the latter one includes much more interface modes than the SL-ROM, ML1-ROM, and ML2-ROM.

An eigenfrequency comparison is usually carried out in conjunction with a comparison of the associate mode shapes. One commonly used method for comparing mode shape vectors is the modal assurance criterion (MAC) [40]. When the mode shape vectors are mass normalized, it is more appropriate to use the mass weighted MAC, which computes the vector correlation between a pair of mode shapes from the full model  $\Phi_{i,\text{full}}$  and ROM  $\Phi_{j,\text{red}}$  as

$$\text{MAC}_{ij} = \frac{|\Phi_{i,\text{full}}^T M \Phi_{j,\text{red}}|^2}{(\Phi_{i,\text{full}}^T M \Phi_{i,\text{full}})(\Phi_{j,\text{red}}^T M \Phi_{j,\text{red}})} \quad (32)$$

Along the diagonal terms, one finds the matching modes; whereas the offdiagonal terms show the correlation between nonmatching modes. Ideally, matching mode shapes should have a MAC value close to one, whereas cross-correlating different mode shapes should give a value close to zero. The relative mode error  $\epsilon_i$  of the  $i$ th mode  $\Phi_{i,\text{red}}$  is thus calculated based on the matching modes as



a) First 30 eigenfrequencies

$\epsilon_i = 1 - \text{MAC}_{ii}$ . The relative mode errors of the interface ROMs are shown in Fig. 7. The SL-ROM, ML1-ROM, and ML2-ROM all yield good results for the first 30 modes. Although the LL-ROM contains more interface modes in the reduction basis, the error for the LL-ROM is substantial for the higher-frequency modes.

**B. NACA Airfoil Wing-Box Structure**

We consider here a thin-walled wing-box structure proposed in [39] and shown in Fig. 8. The cross section features a NACA 0012 profile; the structure is stiffened with ribs along the chord direction and spars along the longitudinal direction. The structure is meshed with triangular flat shell elements with six DOFs per node, resulting in 135,570 DOFs and 49,968 elements for the full model. The Young modulus is  $E = 70$  GPa, the Poisson' ratio is  $\nu = 0.33$ , and the density is  $\rho = 2700$  kg/m<sup>3</sup>. A uniform thickness of 1.5 mm is adopted across the whole structure. The wing has a total length of 5 m and is cantilevered at one end. The significantly large number of DOFs of the full model allows us to appreciate the computational advantages associated to interface reduction. In Fig. 8a, the pressure load has been applied at the highlighted area. In Fig. 8b, the skin panels have been removed for a clear view, and the tip node is highlighted. In Fig. 8c, the wing-box structure has been divided into 600 substructures. In Fig. 8d, the first 25 substructures associated to one wing section has been plotted. In Fig. 8e, 600 substructures are evenly grouped into four subsets for multilevel interface reduction.

The wing box is then divided into 600 substructures, connected through 792 interface sets. The subdivision of the wing-box structure

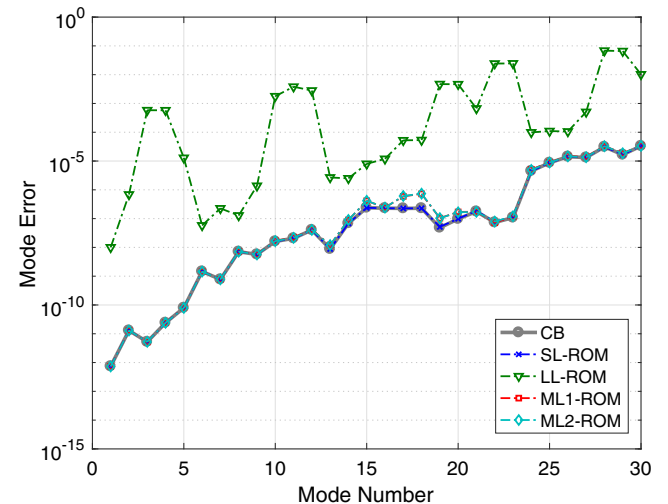
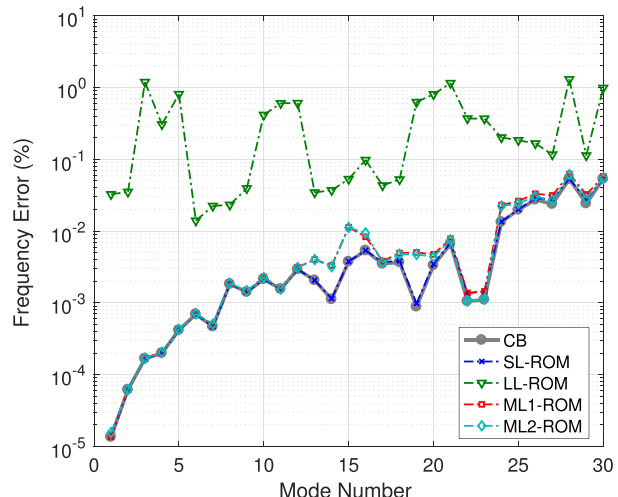


**Fig. 7** Relative mode error of the ROMs as compared to the full model.



b) Relative error for the first 30 frequencies

**Fig. 6** First 30 eigenfrequencies and the corresponding relative errors of the CB-ROM, SL-ROM, LL-ROM, ML1-ROM, and ML2-ROM.

Downloaded by TU DELFT on July 23, 2020 | http://arc.aiaa.org | DOI: 10.2514/1.1056196

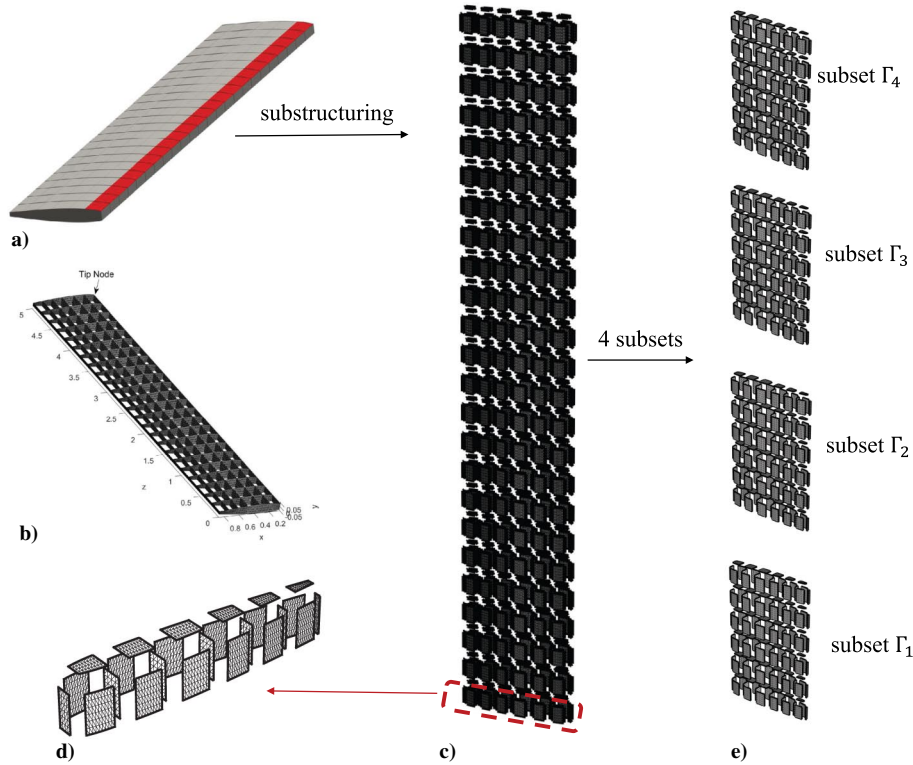


Fig. 8 Illustration of the wing-box structure.

is illustrated in Fig. 8c. Note that this subdivision can in fact reflect a common industrial scenario, where rather detailed FE models of each component might exist for component sizing and stress analysis. The DOFs of the full model are split into  $n_{CB}^B = 28,944$  interface DOFs and  $n_G^I = 106,626$  internal DOFs. We first investigated the accuracy of the frequency and mode of the assembled systems using different interface reduction techniques. The linear response of the wing box is analyzed when a spatially uniform, multiharmonic pressure load is applied locally on the structure skin at an area highlighted in Fig. 8a. The dynamic load function is given as

$$f(t) = 1000 \sum_{i=1}^{15} \left(1 - \frac{(i-1)^2}{392}\right) \sin(\omega_i \times t), \quad \text{with } \omega_i = 250 \times \left(\frac{i}{15}\right)^2 \quad (33)$$

The number of retained IVMs for each substructure is determined by a frequency cutoff criterion: only IVMs associated to frequencies lower than 1500 Hz are kept in the reduced-order basis (ROB) of each substructure. The CB-ROM therefore reduces the internal DOFs from  $n_G^I = 106,626$  to  $m_{CB}^I = 1440$ . The SL-ROM is built with the same frequency cutoff criterion by including the SCC modes  $\tilde{\Phi}_{SC}^B$  associated to frequencies lower than 1500 Hz. This results into keeping the first  $m_{SC}^B = 1170$  SCC modes in the final reduction basis. As for the ML1-ROM and ML2-ROM, all the substructures are collected into four subsets ( $\Gamma_1$  to  $\Gamma_4$ ), as shown in Fig. 8e. The same frequency cutoff criterion is again used here. For the ML1-ROM, the interface DOFs are further reduced by replacing the  $n_{CB}^B = 28,944$  CMs with the first  $m_{\Gamma_i}^N = 168$  interface-level IVMs  $\tilde{\Phi}_{\Gamma_i}^{NN}$  for subset ( $\Gamma_1$  to  $\Gamma_3$ ), as well as  $m_{\Gamma_4}^N = 180$  interface-level IVMs for subset  $\Gamma_4$  together with the first  $m_{\Gamma_i}^C = 153$  interface-level CC modes  $\tilde{\Phi}_{\Gamma_i}^{CC}$ . This results in shrinking the interface DOFs from 28,944 to 837. For the ML2-ROM, the internal DOFs of each subset are reduced by using  $m_{\Gamma_i}^M = 369$  merged IVMs  $\tilde{\Phi}_{\Gamma_i}^M$  for subset ( $\Gamma_1$  to  $\Gamma_3$ ) and  $m_{\Gamma_4}^M = 373$  merged IVMs for subset  $\Gamma_4$ . The number of CDOFs are reduced by including the first  $m_{\Gamma_i}^C = 153$  interface-level CC modes  $\tilde{\Phi}_{\Gamma_i}^{CC}$ . It will result in 1480 internal DOFs and 153 interface DOFs in total for the ML2-ROM. The LL-ROM is constructed by replacing the CMs in

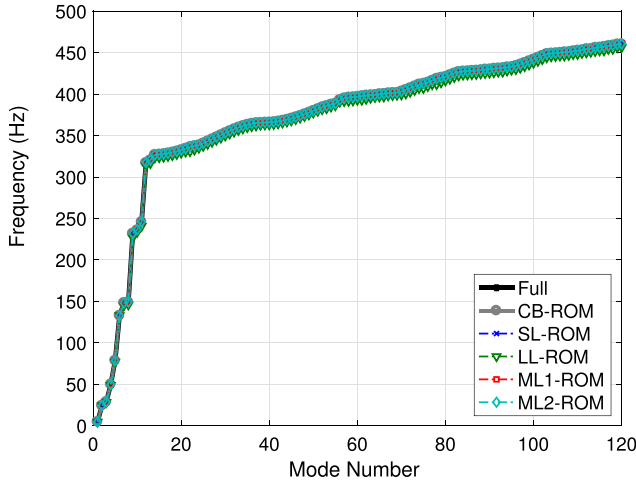
each substructure with the LCC modes  $\tilde{\Phi}_{LCC(s)}$  up to 1500 Hz in each subsystem. Given the large number of substructures and interface sets, the LL-ROM will result in a large number of LCC modes. By using a SVD for each interface set to guard against ill conditioning and using the threshold discussed previously, finally, 22,716 interface modes are retained in the reduction basis. For illustration, the number of modal coordinates of the different ROMs is summarized in Table 3.

The first 120 eigenfrequencies and corresponding relative errors are shown in Fig. 9. The mode shape error is also presented in Fig. 10. As indicated in Figs. 9b and 10, the SL-ROM, ML1-ROM, and ML2-ROM can all lead to a good approximation by keeping the relative frequency error below 0.5% for the first 120 frequencies (up to 460 Hz). The SL-ROM has slightly better accuracy when compared to the ML1-ROM and ML2-ROM, especially at the frequency range of the applied load function (0–250 Hz). The LL-ROM fails to provide a satisfactory frequency approximation, although it includes 22,716 interface modes.

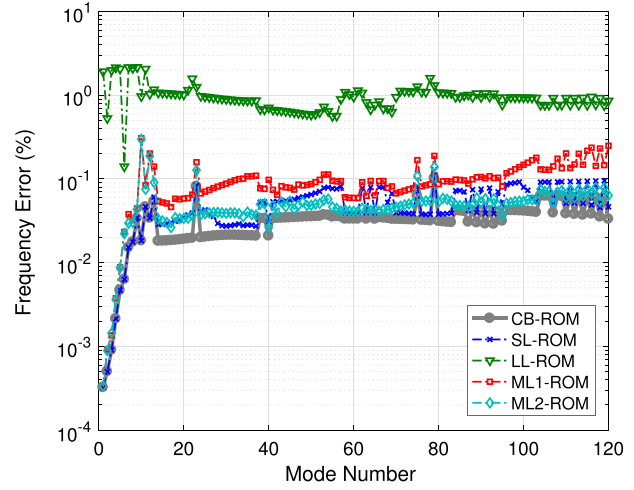
The time history of the displacement for the nodes on the tip node in Fig. 8b is shown in Fig. 11. In addition, we also show the root mean square (RMS) error  $\epsilon_{RMS}$  at an arbitrary time step  $t_i$  defined as

Table 3 Number of modal coordinates of the wing-box model for different ROMs

ROMs	Number of modal coordinates		Total DOFs
CB-ROM	$q_{CB}^B$ 28,944	$\eta_{CB}^I$ 1440	$\text{col}(q_{CB}^B, \eta_{CB}^I)$ 30,384
SL-ROM	$\eta_{SC}^B$ 1170	$\eta_{CB}^I$ 1440	$\text{col}(\eta_{SC}^B, \eta_{CB}^I)$ 2610
LL-ROM	$\eta_{LCC}^B$ 22,716	$\eta_{CB}^I$ 1440	$\text{col}(\eta_{LCC}^B, \eta_{CB}^I)$ 24,156
ML1-ROM	$\eta_{\Gamma_i}^C$ 153	$\eta_{\Gamma_i}^N$ 684	$\eta_{CB}^I$ 1440
			$\text{col}(\eta_{\Gamma_i}^C, \eta_{\Gamma_i}^N, \eta_{CB}^I)$ 2277
ML2-ROM	$\eta_{\Gamma_i}^C$ 153	$\eta_{\Gamma_i}^M$ 1480	$\text{col}(\eta_{\Gamma_i}^C, \eta_{\Gamma_i}^M)$ 1633



a) First 120 eigenfrequencies



b) Relative error for the first 120 frequencies

Fig. 9 First 120 eigenfrequencies and the corresponding relative error of the CB-ROM, SL-ROM, LL-ROM, ML1-ROM, and ML2-ROM.

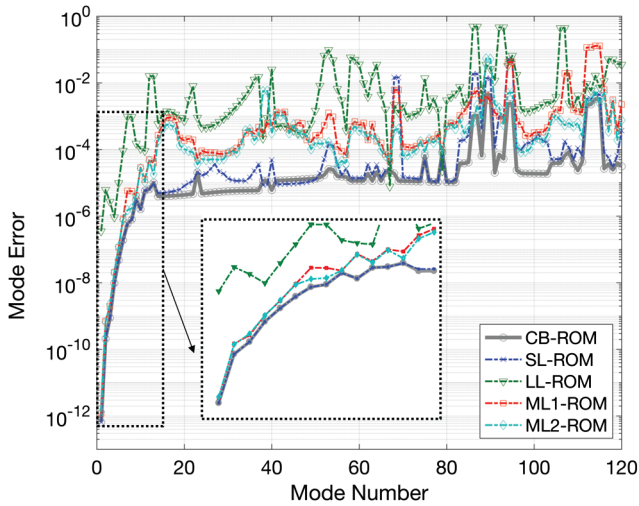


Fig. 10 Relative mode error of the ROMs as compared to the full model.

$$\begin{aligned} \epsilon_{\text{RMS}}(t_i) &= \sqrt{\frac{1}{n} (\|q_x(t_i) - \bar{q}_x(t_i)\|^2 + \|q_y(t_i) - \bar{q}_y(t_i)\|^2 + \|q_z(t_i) - \bar{q}_z(t_i)\|^2)} \end{aligned} \quad (34)$$

where  $q_x, q_y, q_z$  and  $\bar{q}_x, \bar{q}_y, \bar{q}_z$  are the  $x, y, z$  components of the node displacement from the full and ROMs, respectively (rotational DOFs are excluded).

As observed in Fig. 11, although the LL-ROM is inaccurate, all the other interface reduction techniques are able to reproduce the full solution. The RMS error better highlights the difference in performance between the various methods. It can be noticed that the SL-ROM can reproduce the full solution as accurately as the CB-ROM (i.e., without interface reduction). Although the ML1-ROM and ML2-ROM can both produce a satisfactory approximation, the accuracy of the ML2-ROM is slightly better than that of the ML1-ROM.

### C. Computational Efficiency

The computational complexity of the different interface reduction methods has been discussed in detailed in Sec. V. In this subsection, we compare the computational time required by each of the methods proposed. All simulations are performed in MATLAB®R2015, on the Delft University of Technology’s Precision and Microsystems Engineering cluster, equipped with eight-core Intel® Xeon® CPUs (E5-2630v3) at 2.4 GHz and with 128 GB of RAM.

Table 4 compares the computational cost for the wing-box structure in Sec. VI.B. The complexity comparisons have been split into three parts: 1) the construction of the reduction basis for different substructuring methods, which are done *offline*; 2) the frequency analysis of the assembled system; and 3) the transient analysis of the response solution, which would be regarded as an *online* analysis. Obviously, the full analysis does not carry any offline costs. The reduction basis for each substructure and each subset can be parallelized. Note that, in this particular example, the same substructures and subsets are instanced many times along the structure, so one needs to compute the reduction basis only once for each repeated set. In a more general case, because of the possibility of parallelization, the computational cost is mainly dependent on the most time-consuming subsystems or subsets; see Table 1. The computational efficiency is measured by the speedup factor, which is defined as

$$S = \frac{C_{\text{on}} t_{\text{full}}}{C_{\text{off}} t_{\text{off}} + C_{\text{on}} t_{\text{on}}}, \quad \text{with } C_{\text{off}} + C_{\text{on}} = 1 \quad (35)$$

The offline calculation cost is neglected by setting  $S_1: C_{\text{off}} = 0, C_{\text{on}} = 1$ . The so obtained speedup factor  $S_1$  is justified when the same ROM is used for many different load cases. Alternatively, one can set an equal weightage to offline and online costs, i.e.,  $S_2: C_{\text{off}} = 0.5, C_{\text{on}} = 0.5$ . This covers the limit case in which the ROM is used only once. In addition, the accuracy of different ROMs is measured in terms of global relative errors (GREs) by defining

$$\text{GRE}_\diamond = \frac{\sqrt{\sum_t [q_\diamond(t) - \bar{q}_\diamond(t)]^T [q_\diamond(t) - \bar{q}_\diamond(t)]}}{\sqrt{\sum_t q_\diamond(t)^T q_\diamond(t)}} \times 100\% \quad (36)$$

where the subscript  $\diamond$  designates the displacement of the full solution  $q$  and reduced solution  $\bar{q}$  in the  $x, y,$  and  $z$  directions, respectively.

The computational time of the frequency analysis and transient analysis cannot be significantly reduced by the CB-ROM, although the internal DOFs are greatly reduced. In this wing-box example, the size of the interface and internal DOFs is comparable, and therefore the system matrices of the CB-ROM still contain a large number of interface DOFs.

From the results shown in Table 4, one can see that all interface reduction methods do deliver a slight advantage with respect to the CB-ROM for frequency analysis, when offline cost is considered to compute the speed-up factor. In particular, for this specific case, the ML1-ROM and ML2-ROM cut the computation time of the frequencies by factors of  $(46.5 + 1.7)/(1.79 + 24.51) = 1.83$  and  $(46.5 + 1.7)/(34.98 + 0.86) = 1.34$  respectively. The LL-ROM provides similar figures, but it was shown to be inaccurate. The

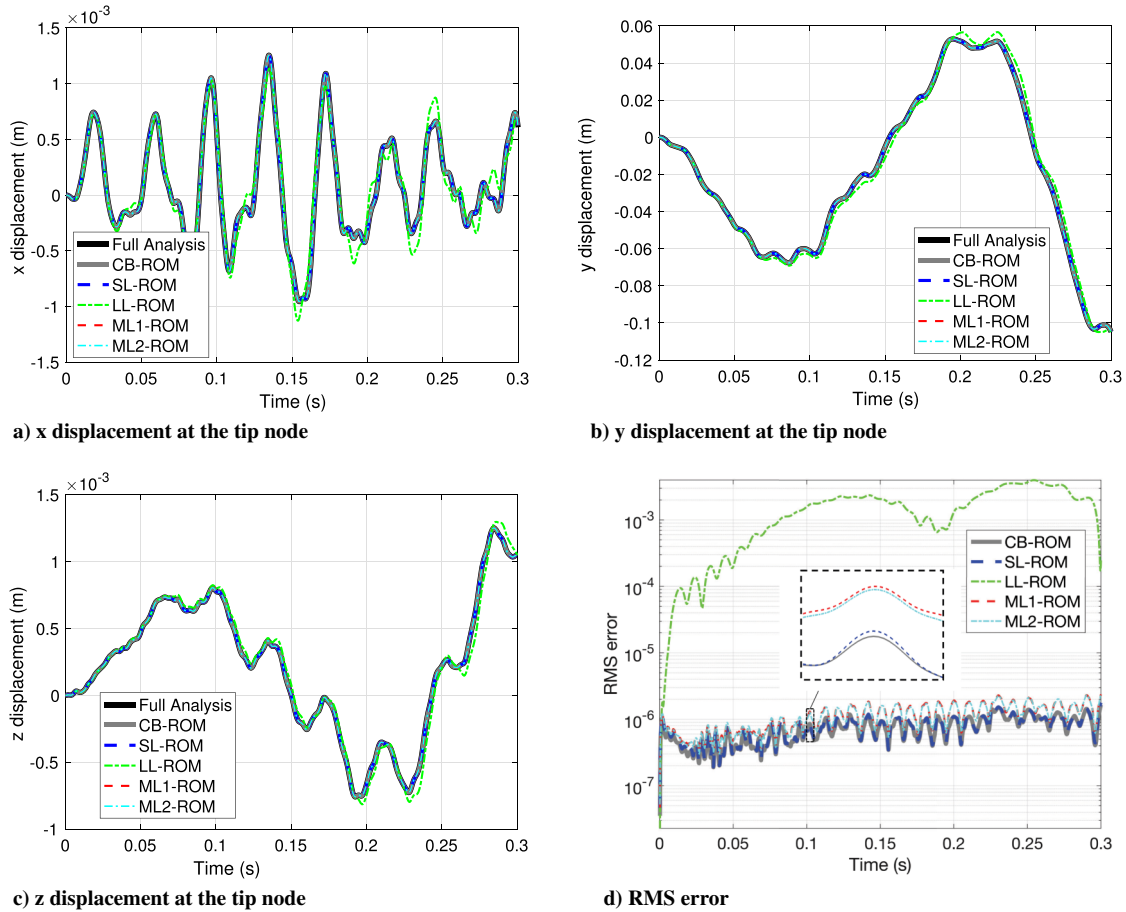


Fig. 11 Time history of solution (displacement) in x, y, and z directions at the tip node of the wing-box structure and the corresponding RMS error.

SL-ROM, on the contrary, required large offline computations, and therefore was not competitive against the CB-ROM.

The major advantage in performing interface reduction comes, in fact, when a transient analysis is needed, as can be seen by looking at the speedup factors reported in Table 4. It is emphasized here that the final size of the ROMs, and therefore the computational savings, depends on the cutoff criterion previously introduced in Sec. VI.B. In this respect, the ML2-ROM features the smallest size, and therefore results in the best speedup factor  $S_1$  of 10.93. In both the ML1-ROM and ML2-ROM, the offline computational cost can be reduced by setting up smaller, parallelizable problems relative to each subset, and the frequency analysis and online (transient analysis) computational cost are reduced, owing to the final system matrices with much smaller sizes.

The GRE is also shown in Table 4. The SL-ROM offers a reduced solution almost as accurate as the CB-ROM. The LL-ROM, on the other side, is largely inaccurate. The multilevel interface reduction methods ML1-ROM and ML2-ROM still guarantee good accuracy while increasing the speed. In particular, the ML2-ROM is more accurate, and faster, than the ML1-ROM, but it requires larger offline

calculations. It should also be noted here that the obtained results for the ML1-ROM and ML2-ROM depend on the subset division. An attempt at finding the best division to maximize the speedup is not made in this work.

Although the ML1-ROM and ML2-ROM are clear winners for the case discussed here, the selection of the “best” interface reduction method is somewhat problem dependent. Here, we attempt to give guidelines by making the following observations.

1) For the SL-ROM, the system-level interface reduction is preferred when high accuracy is required and the offline cost can be neglected, i.e., the speedup factor  $S_1$  is justified. Therefore, the SL-ROM is suitable for problems in which the size of the interface DOFs is moderate, and the ROM needs to be constructed only once.

2) For the LL-ROM, although its accuracy is the worst when compared to its counterparts, the LL-ROM is still an option if one is interested in the low-frequency spectrum of systems featuring a limited number of substructures, which are connected through simple patterns, such as the double- $\square$ -shaped FE model discussed in Sec. VI.A. Therefore, the LL-ROM may be applied for relatively simple systems during the design process, when design changes

Table 4 Computational time of wing-box structure for the CB-ROM, SL-ROM, LL-ROM, ML1-ROM, and ML2-ROM

	Computational time, s					
	Full	CB-ROM	SL-ROM	LL-ROM	ML1-ROM	ML2-ROM
ROB construction (offline)	—	1.70	578.13	6.17	24.51	34.98
Frequency analysis	74.88	46.50	3.51	27.60	1.79	0.86
Transient analysis (online)	387.20	200.80	120.10	113.69	53.35	35.42
Speedup factor $S_1$	—	1.92	3.22	3.41	7.26	10.93
Speed up factor $S_2$	—	1.91	0.55	3.23	4.85	5.50
GRE <sub>x</sub> , %	—	0.0466	0.0506	28.86	0.1112	0.1058
GRE <sub>y</sub> , %	—	0.0033	0.0034	8.10	0.0050	0.0049
GRE <sub>z</sub> , %	—	0.0050	0.0052	10.09	0.0162	0.0149

occur in some parts of the structure; thus, the ROM has to be frequently rebuilt. The LL-ROM benefits from a cheap offline cost. However, it is not applicable when the substructures are connected through numerous interfaces because the method does not properly consider the contributions of neighboring subcomponents.

3) For the ML1-ROM and ML2-ROM, these two methods provide good speedup and accuracy for both frequency and transient analyses. Therefore, they are applicable for problems where both accuracy and computational efficiency are of concern. They are suitable for the design process when changes occur within a few local subsets. In this case, only the ROB's relative to the modified parts need to be rebuilt. The ML2-ROM is more accurate and faster (online) than the ML1-ROM, at the price of a slightly increased offline cost.

## VII. Conclusions

The multilevel interface reduction techniques are proposed for complex systems featuring multiple subcomponents and a large number of interface DOFs. The main idea is to group subcomponents into different subsets and perform a secondary CB reduction for the resulting subset DOFs. The methods localize the interface reduction by applying a multilevel static condensation and eigenvalue analysis on each subset in parallel. As opposed to a traditional local-level technique, the proposed methods better consider the interaction between interfaces. Because of this, the techniques advocated provide accuracy comparable to system-level interface reduction methods. At the same time, the proposed techniques enable computational time savings by setting up smaller, parallelizable problems relative to each subset. Two variants of the multilevel interface reduction techniques (ML1-ROM and ML2-ROM) are investigated. In the ML1-ROM, a secondary CB reduction is performed for the interface DOFs of each subset. In the ML2-ROM, the same CB reduction is performed for all DOFs of each subset. The methods of both eigenvalues calculations and numerical time integration are assessed. When a frequency cutoff criterion is applied for the selection of modes, the ML2-ROM results in a smaller (and therefore faster) and more accurate ROM. This comes at the expense of a slightly larger offline cost.

All the interface reduction techniques have been tested for the rather complex numerical examples featuring several subcomponents and large meshes. The proposed multilevel methods outperformed the system-level interface reduction in terms of achievable speedup while delivering comparable accuracy. It was indicated that the multilevel methods were particularly useful when dealing with systems featuring large and multiconnected interfaces. In cases of simpler and smaller interfaces, guidelines were provided for the choice of the most suited reduction method.

The methods proposed are particularly suited for complex industrial cases for which detailed, and therefore large, FE models of subcomponents are required for simulation. The application of the proposed ROMs (ML1-ROM and ML2-ROM) is straightforward because the methods rely on existing well-known reduction techniques, which are combined in a novel fashion.

## References

- [1] Klerk, D. D., Rixen, D. J., and Voormeeren, S. N., "General Framework for Dynamic Substructuring: History, Review and Classification of Techniques," *AIAA Journal*, Vol. 46, No. 5, 2008, pp. 1169–1181. doi:10.2514/1.33274
- [2] Hurty, W. C., "Vibrations of Structural Systems by Component Mode Synthesis," *Journal of the Engineering Mechanics Division*, Vol. 86, No. 4, 1960, pp. 51–70.
- [3] Hurty, W. C., "Dynamic Analysis of Structural Systems Using Component Modes," *AIAA Journal*, Vol. 3, No. 4, 1965, pp. 678–685. doi:10.2514/3.2947
- [4] Bampton, M. C. C., and Craig, J. R. R., "Coupling of Substructures for Dynamic Analyses," *AIAA Journal*, Vol. 6, No. 7, 1968, pp. 1313–1319. doi:10.2514/3.4741
- [5] Craig, R. R., "Coupling of Substructures for Dynamic Analyses: An Overview," *AIAA/ASME/ASCE/AHS/ASC Structures, Structural Dynamics, and Materials Conference and Exhibit*, AIAA Paper 2000-1573, 2000.
- [6] Craig, R. R., Jr., and Chang, C.-J., "Substructure Coupling for Dynamic Analysis and Testing," NASA TR CR-2781, 1977, <https://ntrs.nasa.gov/search.jsp?R=19770010568>.
- [7] Castanier, M. P., Tan, Y.-C., and Pierre, C., "Characteristic Constraint Modes for Component Mode Synthesis," *AIAA Journal*, Vol. 39, No. 6, 2001, pp. 1182–1187. doi:10.2514/2.1433
- [8] Hong, S.-K., Epureanu, B. I., and Castanier, M. P., "Next-Generation Parametric Reduced-Order Models," *Mechanical Systems and Signal Processing*, Vol. 37, Nos. 1–2, 2013, pp. 403–421. doi:10.1016/j.ymssp.2012.12.012
- [9] Lindberg, E., Hörlin, N.-E., and Göransson, P., "Component Mode Synthesis Using Undeformed Interface Coupling Modes to Connect Soft and Stiff Substructures," *Shock and Vibration*, Vol. 20, No. 1, 2013, pp. 157–170. doi:10.1155/2013/262354
- [10] Tran, D. M., "Component Mode Synthesis Methods Using Interface Modes. Application to Structures with Cyclic Symmetry," *Computers and Structures*, Vol. 79, No. 2, 2001, pp. 209–222. doi:10.1016/S0045-7949(00)00121-8
- [11] Tran, D.-M., "Component Mode Synthesis Methods Using Partial Interface Modes: Application to Tuned and Mistuned Structures with Cyclic Symmetry," *Computers and Structures*, Vol. 87, Nos. 17–18, 2009, pp. 1141–1153. doi:10.1016/j.compstruc.2009.04.009
- [12] MacNeal, R. H., "Special Issue on Structural Dynamics a Hybrid Method of Component Mode Synthesis," *Computers and Structures*, Vol. 1, No. 4, 1971, pp. 581–601. doi:10.1016/0045-7949(71)90031-9
- [13] Rubin, S., "Improved Component-Mode Representation for Structural Dynamic Analysis," *AIAA Journal*, Vol. 13, No. 8, 1975, pp. 995–1006. doi:10.2514/3.60497
- [14] Rixen, D. J., "A Dual Craig–Bampton Method for Dynamic Substructuring," *Journal of Computational and Applied Mathematics*, Vol. 168, Nos. 1–2, 2004, pp. 383–391. doi:10.1016/j.cam.2003.12.014
- [15] Rixen, D. J., "Force Modes for Reducing the Interface Between Substructures," *Proceedings of IMAC-XX: A Conference on Structural Dynamics, Society for Experimental Mechanics*, Vol. 2, Soc. for Experimental Mechanics, Bethel, CT, 2002, pp. 1–8.
- [16] Aoyama, Y., and Yagawa, G., "Component Mode Synthesis for Large-Scale Structural Eigenanalysis," *Computers and Structures*, Vol. 79, No. 6, 2001, pp. 605–615. doi:10.1016/S0045-7949(00)00165-6
- [17] Herrmann, J., Maess, M., and Gaul, L., "Substructuring Including Interface Reduction for the Efficient Vibro-Acoustic Simulation of Fluid-Filled Piping Systems," *Mechanical Systems and Signal Processing*, Vol. 24, No. 1, 2010, pp. 153–163. doi:10.1016/j.ymssp.2009.05.003
- [18] Balmès, E., "Use of Generalized Interface Degrees of Freedom in Component Mode Synthesis," *Proceedings of the IMAC XIV Conference*, Soc. for Experimental Mechanics, Bethel, CT, 1996, pp. 204–210.
- [19] des Roches, G. V., Bianchi, J.-P., Balmes, E., Lemaire, R., and Pasquet, T., "Using Component Modes in a System Design Process," *Structural Dynamics, Volume 3: Proceedings of the 28th IMAC, A Conference on Structural Dynamics*, Springer, New York, 2011, pp. 617–625.
- [20] Bennighof, J. K., and Lehoucq, R. B., "An Automated Multilevel Substructuring Method for Eigenspace Computation in Linear Elastodynamics," *SIAM Journal on Scientific Computing*, Vol. 25, No. 6, 2004, pp. 2084–2106. doi:10.1137/S1064827502400650
- [21] Lee, S., Mok, H., and Kim, C.-W., "On a Component Mode Synthesis on Multi-Level and Its Application to Dynamics Analysis of Vehicle System Supported with Spring-Stiffness Damper System," *Journal of Mechanical Science and Technology*, Vol. 25, No. 12, 2011, pp. 3115–3121. doi:10.1007/s12206-011-1219-9
- [22] Kim, C., "Analysis of Vibration Levels of Large Structural System with Recursive Component Mode Synthesis Method: Theory and Convergence," *Journal of Mechanical Engineering Science*, Vol. 220, No. 9, 2006, pp. 1339–1345.
- [23] Zhao, R., and Yu, K., "An Efficient Transient Analysis Method for Linear Time-Varying Structures Based on Multi-Level Substructuring Method," *Computers and Structures*, Vol. 146, Jan. 2015, pp. 76–90. doi:10.1016/j.compstruc.2014.08.004
- [24] Jezequel, L., and Seito, H. D., "Component Modal Synthesis Methods Based on Hybrid Models, Part I: Theory of Hybrid Models and Modal Truncation Methods," *Journal of Applied Mechanics*, Vol. 61, No. 1, 1994, pp. 100–108. doi:10.1115/1.2901383

- [25] Besset, S., and Jézéquel, L., "Dynamic Substructuring Based on a Double Modal Analysis," *Journal of Vibration and Acoustics*, Vol. 130, No. 1, 2007, Paper 011008. doi:10.1115/1.2346698
- [26] Monteil, M., Besset, S., and Sinou, J. J., "A Double Modal Synthesis Approach for Brake Squeal Prediction," *Mechanical Systems and Signal Processing*, Vols. 70–71, Supp. C, March 2016, pp. 1073–1084. doi:10.1016/j.ymssp.2015.07.023
- [27] Sinou, J.-J., and Besset, S., "Simulation of Transient Nonlinear Friction-Induced Vibrations Using Complex Interface Modes: Application to the Prediction of Squeal Events," *Shock and Vibration*, Vol. 2017, Jan. 2017, Paper 6107251. doi:10.1155/2017/6107251
- [28] Kuether, R. J., Allen, M. S., and Hollkamp, J. J., "Modal Substructuring of Geometrically Nonlinear Finite-Element Models," *AIAA Journal*, Vol. 54, No. 2, 2016, pp. 691–702. doi:10.2514/1.J054036
- [29] Kuether, R. J., Allen, M. S., and Hollkamp, J. J., "Modal Substructuring of Geometrically Nonlinear Finite Element Models with Interface Reduction," *AIAA Journal*, Vol. 55, No. 5, 2017, pp. 1695–1706. doi:10.2514/1.J055215
- [30] Idelsohn, S. R., and Cardona, A., "A Reduction Method for Nonlinear Structural Dynamic Analysis," *Computer Methods in Applied Mechanics and Engineering*, Vol. 49, No. 3, 1985, pp. 253–279. doi:10.1016/0045-7825(85)90125-2
- [31] Voormeeren, S. N., "Dynamic Substructuring Methodologies for Integrated Dynamic Analysis of Wind Turbines," Ph.D. Thesis, Delft Univ. of Technology, Delft, The Netherlands, 2012.
- [32] Bourquin, F., "Component Mode Synthesis and Eigenvalues of Second Order Operators: Discretization and Algorithm," *ESAIM: Mathematical Modelling and Numerical Analysis*, Vol. 26, No. 3, 1992, pp. 385–423. doi:10.1051/m2an/1992260303851
- [33] Guyan, R. J., "Reduction of Stiffness and Mass Matrices," *AIAA Journal*, Vol. 3, No. 2, 1965, pp. 380–380. doi:10.2514/3.2874
- [34] Gruber, F. M., and Rixen, D. J., "Evaluation of Substructure Reduction Techniques with Fixed and Free Interfaces," *Journal of Mechanical Engineering*, Vol. 62, Nos. 7–8, 2016, pp. 452–462. doi:10.5545/sv-jme.2016.3735
- [35] Golub, G. H., and Van Loan, C. F., *Matrix Computations*, 3rd ed., Vol. 3, Johns Hopkins Univ. Press, Baltimore, MD, 2012, pp. 233–303.
- [36] Holmes, M., Gray, A., and Isbell, C., "Fast SVD for Large-Scale Matrices," *Workshop on Efficient Machine Learning at NIPS*, Vol. 58, 2007, pp. 249–252, [https://www.researchgate.net/publication/228820785\\_Fast\\_SVD\\_for\\_large-scale\\_matrices](https://www.researchgate.net/publication/228820785_Fast_SVD_for_large-scale_matrices).
- [37] Coppersmith, D., and Winograd, S., "Matrix Multiplication via Arithmetic Progressions," *Journal of Symbolic Computation*, Vol. 9, No. 3, 1990, pp. 251–280. doi:10.1016/S0747-7171(08)80013-2
- [38] Geradin, M., and Rixen, D., *Mechanical Vibrations: Theory and Application to Structural Dynamics*, Wiley, New York, 1997, pp. 367–411.
- [39] Jain, S., Tiso, P., Rutzmoser, J. B., and Rixen, D. J., "A Quadratic Manifold for Model Order Reduction of Nonlinear Structural Dynamics," *Computers and Structures*, Vol. 188, Aug. 2017, pp. 80–94. doi:10.1016/j.compstruc.2017.04.005
- [40] Allemang, R. J., and Brown, D. L., "A Correlation Coefficient for Modal Vector Analysis," *Proceedings of the 1st International Modal Analysis Conference*, Vol. 1, Union College Press, Orlando, FL, 1982, pp. 110–116.

R. K. Kapania  
Associate Editor